MCB
Journals.ASM.org

# Dynamic Estrogen Receptor Interactomes Control Estrogen-Responsive Trefoil Factor (TFF) Locus Cell-Specific Activities

**Justine Quintin,[a] Christine Le Péron,[a] Gaëlle Palierne,[a] Maud Bizot,[a] Stéphanie Cunha,[a*] Aurélien A. Sérandour,[a*] Stéphane Avner,[a] Catherine Henry,[b] Frédéric Percevault,[a] Marc-Antoine Belaud-Rotureau,[b,c] Sébastien Huet,[a] Erwan Watrin,[d] Jérôme Eeckhoute,[a,e] Vincent Legagneux,[f] Gilles Salbert,[a] Raphaël Métivier[a]**

Equipe SP@RTE, UMR CNRS 6290, Equipe Labellisée Ligue contre le Cancer, Université de Rennes I, Rennes, France[a]; Cytogenetics and Cellular Biology Department, CHU, Rennes, France[b]; BIOSIT, UMR CNRS 6290, Université de Rennes I, Faculté de Médecine, Rennes, France[c]; Equipe CC, UMR CNRS 6290, Université de Rennes I, Faculté de Médecine, Rennes, France[d]; INSERM U1011, Université Lille-Nord de France, Faculté de Médecine de Lille-Pôle Recherche, Lille, France[e]; Equipe EGD, UMR CNRS 6290, Université de Rennes I, Faculté de Médecine, Rennes, France[f]

**Estradiol signaling is ideally suited for analyzing the molecular and functional linkages between the different layers of information directing transcriptional regulations: the DNA sequence, chromatin modifications, and the spatial organization of the genome. Hence, the estrogen receptor (ER) can bind at a distance from its target genes and engages timely and spatially coordinated processes to regulate their expression. In the context of the coordinated regulation of colinear genes, identifying which ER binding sites (ERBSs) regulate a given gene still remains a challenge. Here, we investigated the coordination of such regulatory events at a 2-Mb genomic locus containing the estrogen-sensitive trefoil factor (TFF) cluster of genes in breast cancer cells. We demonstrate that this locus exhibits a hormone- and cohesin-dependent reduction in the plasticity of its three-dimensional organization that allows multiple ERBSs to be dynamically brought to the vicinity of estrogen-sensitive genes. Additionally, by using triplex-forming oligonucleotides, we could precisely document the functional links between ER engagement at given ERBSs and the regulation of particular genes. Hence, our data provide evidence of a formerly suggested cooperation of enhancers toward gene regulation and also show that redundancy between ERBSs can occur.**

In mammals, gene transcription relies on complex and highly organized regulatory processes, which include binding of transcription factors to cognate DNA sequences (*cis* elements), chromatin structure and epigenetic information, the action of additional factors in *trans* (cofactors and RNA polymerase II [Pol II] machinery), and the spatial organization of the genome (1–5). Signaling pathways initiated by steroid hormones, such as 17β-estradiol (E2), provide model systems to study these different layers of transcription regulation in mammalian cells. Indeed, exposure to estrogens leads to transcriptional changes to cell-specific gene repertoires, which are mediated by E2-bound estrogen receptors (ESR1 [referred to as ER throughout this report] and ESR2) (6). On model gene promoters, such as *TFF1*, ER together with a number of its cofactors associates with cognate binding sites (BSs) in a cyclic manner to direct their transcription (7, 8). The spatial organization of the genome also determines the coordinated expression of genes (9, 10). This is notably the case for ER, where the existence of clusters of coregulated genes can originate from genetic and epigenetic information or from the dynamics of chromatin itself. In some instances, such coordinated regulation of colinear genes depends on a single regulating unit (e.g., *HBB*, *Mrf4*, and *Hox* clusters [11–13]).

Genome-wide analyses of ER binding sites (ERBSs) have demonstrated that ER binds only rarely to the proximal promoter of its target genes but is mobilized onto intergenic and intronic sequences (14), which have been proposed to communicate with target genes via long-distance intrachromosomal interactions (15). Whether these distant elements are acting as global regulators for clustered E2-responsive genes is still an intriguing question. In addition, these genome-wide studies also showed that additional transcription factors are required for the accurate targeting of ER onto cognate sequences along the whole genome (16). These factors include FOXA1 (17), TFAP2C (18), and PBX1 (19). Among those, FOXA1 may act as an allosteric sensor for histone marks associated with active or poised chromatin (such as H3K4 mono- or dimethylation), and it is therefore considered a pioneer factor preparing chromatin for subsequent binding of ER (20–22).

We aimed here to obtain functional and mechanistic evidence that distant ERBS elements actually constitute global regulators for clustered E2-responsive genes. To do so, we engaged an extensive analysis of the mechanisms involved in the coordination of the estrogenic response of one cluster of E2-sensitive genes in breast carcinoma cells. These studies were performed in different breast cancer cell lines: MCF-7 cells that constitutively express both ER and FOXA1 and MDA-MB231 cells that were engineered to constitutively express ER but not FOXA1 (these cells were named MDA::ER cells [23]). Comparative observations made in these two cell lines allowed us to interrogate whether the introduction of ER into MDA-MB231 cells is sufficient to recapitulate the regulatory processes observed in MCF-7 cells at the trefoil factor

**Received** 26 July 2013 **Returned for modification** 3 September 2013
**Accepted** 9 April 2014
**Published ahead of print** 21 April 2014
Address correspondence to Raphaël Métivier, raphael.metivier@univ-rennes1.fr.
* Present address: Stéphanie Cunha, Huntsman Cancer Institute, Salt Lake City, Utah, USA; Aurélien A. Sérandour, CRI, Cancer Research United Kingdom, Cambridge, United Kingdom.
Supplemental material for this article may be found at http://dx.doi.org/10.1128/MCB.00918-13.

doi:10.1128/MCB.00918-13

**TABLE 1** Sequences and characteristics of TFOs

| Target | Sequence | Distance from ERBS center (bp) | Off-target vs specific E value[a] | 35-bp probe sequence[b] |
|---|---|---|---|---|
| MCF-7 cell BS1 | UGGUGTUUGGUUUGGUUGG | 276 | −1.95 (1) | CACAGACGT*GGAAGGAAAGGAATGAGGA*TGATATT |
| MCF-7 cell BS4 | UGGGUGUGUUGGGUCUUGGUUU | 479 | −5.74 (1) | TGACCCT*AAAGGAACAGGGAAGAGAGGGA*TTCAGC |
| MCF-7 cell BS6 | UUUUGUUUGGGUUGGUCUG | 2 | −1.95 (1) | TGGGCACT*GACAGGAAGGGAAAGAAAA*CAGCCTGC |
| MCF-7 cell BS10 | GUUGGUUCGUUGGUGUUU | 248 | −1.98 (1) | GATCTTCCT*AAAGAGGAAGCAAGGAAGC*CAGCCTC |
| MCF-7 cell BS14 | UUGUUCGGUUUGUGGUGG | 511 | −2.02 (2) | GATCTGAT*GGAGGAGAAAGGCAAGAA*CATGTGCGA |
| MCF-7 cell BS16 | GGGGUTGUGGUGGUGGUGUUU | 355 | −5.28 (2) | AGGTGTCC*AAAGAGGAGGAGGAGTAGGGGC*AACAG |
| MDA::ER cell BS1 | UGUUGUUUUGUGGTGGGUG | 371 | −1.98 (1) | CTAGGATGT*GAGGGTGGAGAAAAGAAGAC*GTGAGG |
| MDA::ER cell BS10 | UUUGGGUCGUGUUGGUGG | 273 | −1 (1) | GCAGGAGATG*GAGGAAGAGCAGGGAAA*TAGAAGCT |
| MDA::ER cell BS12 | UGGGUGGTUUUGUGGUGGGGUU | 301 | −5.74 (1) | AGGTGACC*AAGGGGAGGAGAAATGGAGGGA*CATTC |
| Common BS1 | UGGUUUGUUGGGUGUGUGUGUG | 185 | −1.74 (2) | GGAGTTA*GAGAGAGAGGGAAGAAAGGAG*GGGAGGGA |
| Common BS2 | UUUUUUUGUGGGUGGUCGGG | 450 | −3.93 (1) | GGCTGGGGGCAGGAGGGAGAAAAAAATAGTATATA |

[a] Expressed as log[inverse(off target/specific target)]. The numbers in parentheses indicate the number of off targets in the top 5 hits determined from a BLAST analysis (http://blast.ncbi.nlm.nih.gov/).

[b] Nucleotides targeted by the TFOs are in italics. Only the sense oligonucleotide is indicated.

(TFF) locus. The combination of chromosome conformation capture (3C) and circular 3C (4C) methods with chromatin immunoprecipitation (ChIP)-chip experiments and the use of triplex-forming oligonucleotides (TFOs), which allows testing of the functional importance of individual enhancers, defined key molecular features specifying the transcriptional response induced by E2. We show that, in both cell types, ER engages similar mechanisms to regulate transcription of coregulated gene clusters, in particular, through long-range and dynamic interactions between multiple ERBSs and its target genes. By interfering specifically with the association of ER with given ERBSs, we were also able to determine the relative importance of these different BSs in the regulation of corresponding E2-dependent genes.

## MATERIALS AND METHODS

**Reagents.** All chemicals and restriction or modification enzymes were obtained from Sigma, Roche, or New England BioLabs. All primers and small interfering RNAs (siRNAs) were purchased from Sigma. Antibodies were from Abcam, Millipore, or Santa Cruz [actin, catalog no. sc-8432; CTCF, catalog no. 07-729; ER, catalog no. HC20 and ab10(TE111-SD1); FOXA1, catalog no. ab23738; and RAD21, catalog no. ab992]. Anti-Scc1/RAD21 was a gift from J. M. Peters, and the anti-human CAPD2 (anti-hCAPD2) Eg7.2 was previously published (24) Bacterial artificial chromosome (BAC) probes RP11-814F13, CTD-2337B13, RP11-35C4, CTD-260o11, RP11-113F1, and CTD-1033M14 were purchased from Invitrogen.

**TFOs.** We developed a Python algorithm (available upon request) following the rules defined previously (25) to design putative TFOs targeting 15- to 30-bp-long oligopyrimidine-oligopurine tracts included within ERBSs (Table 1) with one possible base divergent from a strict poly(A/G) sequence. Triplex formation was monitored *in vitro* by incubating increasing amounts of TFOs with DNA duplexes for 16 h at 37°C in a buffer containing 10 mM $MgCl_2$, 100 mM NaCl, 50 mM Tris-HCl (pH 7.4), 10% glycerol, and 0.5 mg/ml tRNA. Complexes were separated by native electrophoresis on a polyacrylamide gel containing 10 mM $MgCl_2$ and 50 mM Tris-HCl (pH 7.4) and visualized by methylene blue staining.

**Cell culture and reverse transcription (RT).** MCF-7, MDA-MB231, and MDA-MB231 cells stably expressing ERα (MDA::ER cells [23]) were maintained in Dulbecco modified Eagle medium (DMEM; Gibco) containing 5% fetal calf serum (FCS; BioWest) and antibiotics (Roche) at 37°C under 5% $CO_2$. MDA::ER cell medium was supplemented with 0.8 mg/ml hygromycin (Calbiochem). For experiments requiring treatment with E2, cells were cultivated for 2 days in DMEM without phenol red containing 2% charcoal-stripped FCS (csFCS; BioWest) prior to the addition of E2 (final concentration, $10^{-8}$ M). Total RNAs from $10^7$ cells were purified using the Trizol reagent (Life Technologies, Inc.) according to the manufacturer's instructions. Two micrograms of RNA served as the template for Moloney murine leukemia virus reverse transcriptase (Invitrogen) and Pd(N)6 random hexamers (Amersham Pharmacia Biosciences).

**Transfections.** A total of $2.5 \times 10^6$ cells was plated in 9-cm dishes in DMEM–5% FCS for 16 h and then grown for 24 h in DMEM–2.5% csFCS. The medium was then replaced with 4 ml of FCS and antibiotic-free Opti-MEM (Sigma), and 1 μmol siRNAs (sense; luciferase, AACACUUACGC UGAGUACUUCGA; CTCF, GGAGCCUGCCGUAGAAAUU; RAD21, GGUGAAAAUGGCAUUACGG) or 10 μmol TFOs was then transfected using Oligofectamine, as recommended by the manufacturer (Invitrogen). Following 6 h of incubation, the medium was completed with 125 μl of csFCS, and E2 ($10^{-8}$ M) stimulation was done 36 h later.

**Western blotting.** Half of the cells from confluent 9-cm-diameter dishes were directly lysed in sample buffer and subjected to classical SDS-PAGE. Proteins were transferred onto a Hybond nitrocellulose membrane (Amersham) for 2 h, which was subsequently blocked in phosphate-buffered saline (PBS) or Tris-buffered saline (TBS) complemented with 0.1% Tween 20–4% dry milk for 1 h at 4°C. The membranes were then incubated overnight at 4°C with primary antibodies at appropriate concentrations (CTCF, 1/2,000; Scc1/RAD21, 1/1,000; ER, 1/2,500; FOXA1, 1/2,500; β-actin, 1/5,000; anti-hCAPD2 Eg7.2, 1/2,000). Following three successive washes, the blots were further incubated for 1 h at room temperature using appropriate peroxidase-coupled secondary antibodies diluted 1/10,000 in PBS or TBS plus 0.1% Tween 20–4% dry milk. The proteins in the Western blots were revealed by use of an ECL detection kit (Amersham).

**DNA fluorescence *in situ* hybridization (FISH).** Probes were produced by direct labeling of BAC clones through random priming (Bioprime array CGH genomic labeling system; Invitrogen) using fluorochrome-conjugated nucleotides (dUTP-Alexa Fluor 488 from Invitrogen or dUTP-cyanine 3 from PerkinElmer). Before use, the probes were denatured for 5 min at 80°C and then 30 min at 37°C. Cells were grown for 2 days on glass slides in DMEM without phenol red containing 2.5% csFCS. After addition of $10^{-8}$ M E2 or ethanol (vehicle), slides were washed with PBS and then fixed in 2% paraformaldehyde (PFA) for 10 min at 4°C. PFA-fixed cells were permeabilized in 0.5% Triton X-100 and equilibrated in 1× SSC (1× SSC is 0.15 M NaCl plus 0.015 M sodium citrate) for 5 min. The slides were incubated for 1 h with 20 μg/ml RNase A in 1× SCC at 37°C and then sequentially washed 3 times with PBS and incubated in 2% PFA for 10 min at room temperature, in 100 mM HCl for 10 min, and then in 0.5% Triton X-100 for 10 min, with 3 washings with PBS taking place between each step. The slides were then subjected to denaturation through sequential heating at 73°C in 70% formamide–30% 2× SSC for 7 min and then for 3 min in 50% formamide–50% 2× SSC.

Hybridization with 600 ng of labeled denatured DNA probes was performed overnight at 42°C in hybridization buffer (per 800 μl, 200 μl 25% dextran sulfate, 100 μl 20× SSC, 500 μl deionized formamide) containing 150 μg of Cot-I (Invitrogen) and 150 μg of salmon sperm DNA. The slides were rinsed three times in 2× SSC, in 50% formamide–50% 2× SSC for 20 min at 42°C, and three times in 2× SCC again. Nuclei were stained with DAPI (4′,6-diamidino-2-phenylindole) in 2× SSC for 5 min, and then the slides were mounted with on a coverslip (22 by 40 mm) ProLong Gold antifade reagent (Invitrogen).

**Cytogenetic analysis.** MCF-7 and MDA cells were plated in Lab-Tek chamber slides (Nunc Thermo Scientific) and observed daily until they reached a stage of active division. Cells were then harvested using a MultiPrep Genie 205 apparatus (Genial Genetics) according to the recommendations of the manufacturer. After R banding, 20 metaphases were captured and analyzed. Complementary analysis using FISH was carried out according to standard procedures as described in reference 26. Slides were analyzed with an epifluorescence microscope (Olympus BX61), and images were captured using Isis software (MetaSystems).

**Microscopy and image analysis.** Images of stacks were obtained with the 63× oil immersion objective of a DMRXA microscope (Leica) or with a Zeiss apotome microscope (63× objective). Measurements of the nuclear area and the distance between the centroid of each probe were performed with ImageJ software (http://rsbweb.nih.gov/ij/). Distances were determined in two dimensions (2D), since pilot experiments did not provide any evidence of a qualitative difference between 2D and three-dimensional (3D) FISH experiments (data not shown). Images of entire stacks were taken for all selected nuclei (nonmitotic nuclei and nuclei containing the expected 3 pairs of hybridization signals), and the three channels (red, green, and blue) were isolated using a DeInterleave plug-in. Pictures of *z* stacks (distance, 0.3 μm) containing maximum red or green signal intensities were selected for all channels, merged, and then thresholded to eliminate the background from specific signals for distance measurements. We used pictures of the DAPI (blue) channel to consistently determine the nucleus area, which was calculated following the determination of a threshold fluorescence value corresponding to an entry transition into the nucleus. This value was manually determined as the inflection point of a profile plotting the DAPI signal measured in a 10-pixel large longitudinal window crossing the nucleus against the pixel distance. Images from up to 100 nuclei were analyzed in each experiment. Significant variations between experimental conditions were tested by use of a Fisher *t*-test comparison for unpaired data, with a significance threshold of a *P* value of $\leq 0.05$ being set. To calculate 3D volumes, we first automatically segmented the three-dimensional hybridization signals for each of the color channels using the triangle algorithm (27) implemented in ImageJ. After a cleaning step consisting of the successive application of an opening and closing filter, the 3D volumes of the structures resulting from the union of the two segmentation masks were measured and expressed as voxels. To analyze the results of the kinetic FISH experiment, we had to develop a custom Matlab (MathWorks, Natick, MA) image-processing routine in order to quantitatively analyze the high number of images. For that, we used the maximum-intensity projections of the three-dimensional stacks acquired by fluorescence microscopy. The analysis steps were performed automatically to avoid potential bias associated with manual intervention. The nuclei were segmented on the DAPI channel using the Otsu approach (28), and a watershed algorithm (29) was applied to separate touching nuclei. For detecting the fluorescence spots on the images corresponding to each FISH probe, we used the algorithm developed by Sbalzarini and Koumoutsakos (30). A first filtering step was performed to remove the very dim spots and those located outside the nuclei. The intensities of the remaining spots were estimated and subtracted from the local background. We kept only the spots whose intensities exceeded the threshold TI, which was calculated as follows: $\langle I \rangle + n \times \sigma I$, where $\langle I \rangle$ and $\sigma I$ are the mean and the standard deviation of the spot intensities, respectively, and *n* is a user-defined integer. FOR a subset of images, we compared the spots detected by the automatic analysis and those selected by manual inspection. By setting *n* equal to 5, we optimized the matching between the automatic and manual selections. The spots whose intensities corresponded to the two FISH probes were paired on the basis of a nearest-neighbor criterion. FISH pair distances exceeding 20 pixels were not considered. We noted that our approach was robust toward the choice of the integer *n*, as similar distance distributions were obtained for $3 < n < 7$.

**Microarray and mRNA profiling data analyses.** RNAs for microarray analysis were isolated from $20^7$ MCF7 or MDA::ER cells treated with E2 or ethanol as a vehicle control using an RNeasy Plus minikit (Qiagen) with homogenization through a QIAShredder homogenizer (Qiagen). The integrity and purity of the RNAs were controlled on an Agilent Bioanalyzer using an RNA 6000 Nano assay (Agilent). Ten micrograms of selected samples exhibiting an RNA integrity number (RIN) of >9.8 was then subjected to cDNA synthesis using a SuperScript double-stranded cDNA synthesis kit (Invitrogen) and a mix of 50 pmol of random hexamers and 50 pmol of oligo(dT). cDNAs were then treated for 10 min at 37°C with 5 μg RNase A (Invitrogen), purified through a phenol-chloroform-isoamyl alcohol extraction on Phase Lock light gels (Fisher Scientific), and then precipitated. Following a quality control on agarose-ethidium bromide gels, all subsequent steps (labeling of cDNA, hybridization, and scanning of the arrays) were performed at the NimbleGen service facilities (Reykjavik, Iceland). For each experimental condition, three arrays (NimbleGen *Homo sapiens* 385K array) were hybridized with independently prepared pools of cDNAs synthesized from experimental triplicates (independent experimental and biological triplicates). Quantile normalization of the data through the robust multiarray average (RMA) algorithm and all primary analyses were performed using the ArraySTar software suite (DNAstar, Inc.). Data were filtered according to two criteria: (i) expression values greater than the first quartile in all samples of at least one triplicate and (ii) triplicate standard deviations lower than the third quartile in all triplicate experiments. Experimental groups were compared by analysis of variance (*t* test), and *P* values were adjusted by the Benjamini and Hochberg method (31). Genes were considered differentially expressed between two experimental conditions when their adjusted *P* value was less than 0.05 and the fold change in expression was greater than 1.8. Estrogen-sensitive clusters were then defined by sliding a window of variable sizes and counting the number of E2-regulated genes within these windows. Using this methodology, we empirically determined clusters to be defined as genomic regions comprising at least 3 regulated genes within a window of 7 genes.

**FAIRE assays.** The formaldehyde-assisted isolation of regulatory element (FAIRE) (32) methodology was conducted as described previously (22).

**Chromatin immunoprecipitation.** Cells were washed twice with PBS and cross-linked for 10 min at room temperature using 1.5% formaldehyde (Sigma) diluted in PBS. Following a subsequent incubation with 0.125 M glycine for 2 min, the cells were collected in 1 ml collection buffer (100 mM Tris-HCl [pH 9.4], mM dithiothreitol). Cells were then washed in 1 ml PBS, lysed for 15 min at room temperature in 300 μl of lysis buffer (10 mM EDTA, 50 mM Tris-HCl [pH 8.0], 1% SDS, 0.5% Empigen BB detergent [Sigma]), and chromatin sonicated for 14 min using a BioRuptor apparatus (Diagenode) with duty cycles of 30 s on/30 s off. Chromatin was then cleared through a 10-min centrifugation at 10,000 × *g*. ChIP experiments were then conducted by use of some modifications of a previously described protocol (7) using 1/10 of the chromatin samples (30 μl) of the supernatants as the input, and the remainder was diluted 5-fold in IP buffer (2 mM EDTA, 100 mM NaCl, 20 mM Tris-HCl [pH 8.1], 0.5%Triton X-100). One-fourth of this fraction was subjected to immunoprecipitation overnight after a 3-h preclearing at 4°C with 10 μg *Saccharomyces cerevisiae* tRNA (R8505; Sigma) and 80 μl of a 50% protein A-Sepharose bead (Amersham Pharmacia Biosciences) slurry. Complexes were recovered after 3 h incubation at 4°C with 5 μg yeast tRNA and 40 μl of protein A-Sepharose. Precipitates were then serially washed using 300 μl of washing buffer (WB) I (2 mM EDTA, 20 mM Tris-HCl [pH 8.1], 0.1% SDS, 1% Triton X-100, 150 mM NaCl), WB II (2 mM EDTA, 20 mM

**TABLE 2** Genomic regions spotted on microarrays

| Chromosome | Genomic coordinate[a] | | Cluster | Regulatory region | Top gene[b] |
|---|---|---|---|---|---|
| | Start | Stop | | | |
| 1 | 16920000 | 18300000 | Yes | MDA::ER cell | *PADI1* |
| 1 | 150450000 | 151200000 | No | MCF-7 cell | *LCE3B* |
| 2 | 118600000 | 123280000 | Yes | MDA::ER cell | *INHBB* |
| 3 | 49890000 | 51600000 | Yes | Both MCF-7 and MDA::ER cells | *SEMA3B* |
| 7 | 72600000 | 73200000 | Yes | MDA::ER cell | *CLDN4* |
| 8 | 67060000 | 68460000 | Yes | MCF-7 cell | *MYBL1* |
| 9 | 138882000 | 139620000 | Yes | MCF-7 cell | *ENTPD2* |
| 10 | 43500000 | 44600000 | No | MCF-7 cell | *CXCL12* |
| 10 | 99800000 | 100130000 | No | MDA::ER cell | *LOXL4* |
| 11 | 1500000 | 3300000 | Yes | MDA::ER cell | *TH3* |
| 11 | 93800000 | 94930000 | Yes | MCF-7 cell | *FUT4* |
| 12 | 9600000 | 10920000 | Yes | MDA::ER cell | *KLRC3* |
| 12 | 14100000 | 16300000 | Yes | MCF-7 cell | *ART4* |
| 14 | 91800000 | 96600000 | Not in MCF-7 cells | Both MCF-7 and MDA::ER cells | *SerpinA1* |
| 16 | 21500000 | 24420000 | Yes | MCF-7 cell | *SCCN1C1* |
| 16 | 54600000 | 55900000 | Yes | MDA::ER cell | *MT1X* |
| 16 | 65600000 | 66240000 | Yes | MDA::ER cell | *HSF4* |
| 17 | 35530000 | 37440000 | Yes | Both MCF-7 and MDA::ER cells | *KRT9* |
| 19 | 54150000 | 54480000 | Yes | MCF-7 | *LHB* |
| 20 | 21000000 | 26800000 | Yes | MDA::ER | *ACSS1* |
| 21 | 36200000 | 47000000 | Yes | Both MCF-7 and MDA::ER cells | *TFF1* |
| 22 | 48720000 | 49380000 | Yes | MDA::ER | *MAPK12* |
| X | 36600000 | 39600000 | Yes | Both MCF-7 and MDA::ER cells | *SYTL5* |

[a] Genomic coordinates are given from the hg18 assembly of the human genome.
[b] The gene exhibiting the most important fold change in expression upon E2 treatment in either MDA::ER or MCF-7 cells.

Tris-HCl [pH 8.1], 0.1% SDS, 1% Triton X-100, 500 mM NaCl), and WB III (1 mM EDTA, 10 mM Tris-HCl [pH 8.1], 1% NP-40, 1% deoxycholate, 0.25 M LiCl) and then twice with 1 mM EDTA, 10 mM Tris-HCl (pH 8.1). Precipitated complexes were removed from the beads through two sequential incubations with 50 μl of 1% SDS, 0.1 M $NaHCO_3$. Cross-linking was reversed by an overnight incubation at 65°C. DNA was purified on NucleoSpin columns (Macherey-Nagel) using 50 μl NTB buffer (Macherey-Nagel). Subsequent quantitative PCR (qPCR) analysis used 1 μl of input material and 3 μl of ChIP samples.

**ChIP-on-chip assays and analysis of published data sets.** The ChIP procedure conducted on chromatin prepared from $15 \times 10^6$ cells was similar to the one described above but with the following modifications for the final steps. Cross-linking was reversed by an overnight incubation at 65°C with 10 μg of proteinase K (Sigma). Following a subsequent incubation of the samples with 2.5 μg RNase (Sigma) for 1 h at 37°C, the DNA was then purified on NucleoSpin columns (Macherey-Nagel) using NTB buffer and eluted in 40 μl of elution buffer. The efficiency of the ChIP assay was then evaluated using qPCR positive and negative controls. Experimental input and ChIP triplicate samples were then pooled by precipitation, resuspended in 25 μl $H_2O$, and divided in two for amplification using a WGA whole-genome amplification kit (Sigma). Following a quality control step, the amplified material was pooled and sent to NimbleGen service facilities (Reykjavik, Iceland) for hybridization on custom 385K arrays. These arrays were conceived by spotting genomic regions containing clusters of E2-regulated genes defined from MDA::ER and MCF-7 cell estrogen-sensitive transcriptomes, as well as regions containing individual control cell-specific estrogen-sensitive genes (Table 2). ChIP-chip signal normalization and peak calling steps were performed using the MA2C algorithm (33) on raw data obtained from two arrays hybridized with DNA prepared in two independent experiments. MA2C parameters were robust normalization (*C* parameter set to 1) and peak calling for a minimum of 4 probes (maximum gap set at 400 bp) in a sliding window with a half width of 300 bp. All binding sites determined in our ChIP-chip experiments were confirmed by independent ChIP-qPCR assays, except for the CTCF BS identified in the TFF1 promoter, which was found to be antibody and experiment dependent. This site was therefore not included in the statistical examination of our data. Published Affymetrix tiling array data (from ER and Pol II ChIP-chip assays performed in MCF-7 cells) were analyzed by model-based analysis of tiling arrays (34). All genomic annotations were performed using algorithms present within the Cistrome web platform (http://cistrome.dfci.harvard.edu/ap) (35). MCF-7 cell ChIP sequencing (ChIP-seq) data for CTCF and RAD21 (concatenation of FASTQ files obtained in duplicate experiments) and the corresponding input were extracted from the GSE25710 series and aligned onto indexed chromosomes of genome hg18 using Bowtie (version 0.12.7) software (36) with parameters $-p$ 7, –best, $-m$ 1, $-n$ 1, –sam, and $-l$ 28. The .sam files were then converted to .wig files, using the SAMtools (version 0.1.12a) (37) and MACS (version 1.3.7.1) (38) programs. To compare the RAD21 ChIP-seq data sets obtained with vehicle- and estradiol-treated cells, we adjusted the bias of diverging sequencing depths through linear normalization (factor, 2.1) of the signal intensities of a given .wig file so as to be comparable to the .wig file with the highest sequencing depth. Peak calling was then performed as previously described (39).

**Triplex capture experiments.** Triplex capture assays were performed on transfected cells, which were subsequently cross-linked by 2% formaldehyde and lysed by sonication as described above. Sonicated chromatin was then incubated for 4 h with streptavidin-coated magnetic beads (Dynal) that were blocked with 10 μg/ml bovine serum albumin (BSA) and 10 μg/ml yeast tRNA for 1 h. Captured DNA was eluted by two rounds of elution in 0.1% SDS, purified following digestion with proteinase K and RNase A, and analyzed by qPCR.

**3C and 4C.** Methods for chromosome conformation capture (3C) and circular 3C (4C) were adapted from those described previously (40) and used the DpnII 4-base cutter as an enzyme of choice. Following a 5-min centrifugation at 2,000 × *g*, aliquots of $2 \times 10^6$ cross-linked cells were washed with 200 μl of 1× DpnII buffer and then lysed overnight at 37°C in 200 μl of 1× DpnII buffer containing 0.3% SDS with shaking. Following 2 passages through a syringe needle, 400 μl of 1× DpnII buffer was sequentially added 4

times, and SDS was sequestered with 67 μl of 20% Triton X-100 at 37°C for 1 h. Fifty microliters of the reaction mixture was then kept as the input fraction for digestion efficiency controls. Five hundred fifty microliters of the chromatin preparation was then digested overnight with 400 U DpnII at 37°C with shaking in a total volume of 500 μl of digestion buffer containing protease inhibitors (Roche). An additional step of 6 h of digestion with 150 U DpnII was then performed. Fifty microliters of the digested chromatin was then kept as a digestion efficiency control, while the remaining was kept at 4°C during this step. To control the digestion efficiency, both input and digested aliquots were incubated with 9.5% SDS for 20 min at 65°C. Cell fragments were then eliminated by centrifugation at 12,000 × *g* for 5 min. TE (Tris-EDTA) buffer (117 μl) was then added together with 5 μl of 10 μg/μl RNase A (Sigma), and the mixture was incubated at 37°C for 30 min before the addition of 8 μl of 5 M NaCl and 10 μl of 10 μg/μl of proteinase K (Sigma). Cross-linking was then reversed overnight at 65°C, and DNA was purified on Macherey-Nagel columns. qPCRs were then performed with the input and digested fractions to calculate the digestion efficiency (*E*; in percent) as follows: $E = 1.9^{CT \text{ input test region} - CT \text{ sample test region}} / 1.9^{CT \text{ input control region} - CT \text{ sample control region}} \times \text{df} \times 100$, where $C_T$ is the threshold cycle, the dilution factor (df) was equal to 0.98360 [(50/610)/(50/600)], and the control region is a region that contains no DpnII fragment. If the value of *E* was >85%, the remaining digested chromatin was subjected to a final lysis step by addition of 108 μl of 10% SDS and incubation at 65°C with shaking for 20 min. Two micrograms of digested chromatin, as evaluated from the amounts of DNA recovered in the digested fraction using a NanoDrop spectrophotometer, was then incubated for 1 h at 37°C with 40 μl of 20% Triton X-100 in a total volume of 694 μl of ligation buffer (10 mM Tris-HCl, pH 7.8, 0.1 μg/μl BSA, protease inhibitors). Ligations for 3C or 4C experiments were then performed at 16°C with gentle agitation for 4 h or 5 days, respectively. For 3C, 10 μl of T4 DNA ligase was added to the reaction mixture together with 80 μl of its buffer, 8 μl of 10 μg/μl BSA, and 8 μl of 100 mM ATP (total volume of 800 μl; DNA concentration = 2.5 ng/μl). For the 4C samples, which required a more diluted concentration of DNA, 906 μl of $H_2O$ was first added and then 160 μl of 10× T4 DNA ligase buffer, 16 μl of 10 μg/μl BSA, 16 μl of 100 mM ATP, and 15 μl of T4 DNA ligase were added (total volume, approximately 1,800 ml). The ligation mix was replenished at days 2 and 4 with ATP (20 μl of 100 mM ATP). Following these 5 days of ligation, 4C samples were further incubated for 1.5 h with 1 μl of T4 DNA ligase in order to ensure that the ligase filled any nicks in the circularized 3C products. The cross-linking of either 3C or 4C DNA products was then reversed overnight at 65°C following the addition of EDTA (final concentration, 1 mM), NaCl (final concentration, 0.2 M), and 10 or 20 μl of 10 μg/μl proteinase K. The samples were then subjected to three successive phenol-chloroform-isoamyl alcohol (25:24:1) extractions, followed by a chloroform washing step, diluted 4 times in water, and precipitated at −20°C for 2 h by 2 volumes of isopropanol. Following centrifugation at 13, 000 × *g*, samples were then washed 3 times with 1 volume of 75% ethanol and resuspended in 50 μl of TE. 3C samples were then processed for analysis. In contrast, the 4C products generated by the 5-day ligation were then purified from linear DNA by a combined digestion with 7 μl of exonuclease I and 2 μl of exonuclease III (New England BioLabs) in a total volume of 100 μl of 1× exonuclease I buffer. Circular DNA was then purified on Macherey-Nagel columns following a 25-min heating step at 85°C to inactivate the enzymes. The elution step was modified by incubating the DNA bound on the columns with 50 μl of Tris-HCl (pH 7.8) containing 20 ng of yeast tRNA for 2 h. 4C libraries were then amplified on a thermocycler using High-Fidelity *Taq* polymerase (Invitrogen) using the following primers: TMPRSS2 (5′-AACATAGTCCTCTTTGGCACA-3′ and 5′-GTCAGTCTCGGGGAGGGACT-3′), RIPK4 (5′-TTGGGAGCTTCCATCAAGAC-3′ and 5′-GCTCCTTCATGGGTTCATTC-3′), TFF3 (5′-GACCAGGGTGTGGTGTCC-3′ and 5′-CAGCTCTGCTGAGGAGTACG-3′), TFF2 (5′-CAGACCCTCATCCTCCAGAC-3′ and 5′TATAAAGGCATCTGGCAATGTG-3′), TFF1 (5′-GCTACATGGAAGGATTTGCTG-3′ and 5′-CAGTGGAGATTATTGTCTCAGA-3′), TMPRSS3 (5′-CATGGCTGCTCTGGGAAC-3′ and 5′CCTCGGCTAAGGAGGTAGAG-3′), and UBASH3A (5′-GTACGGCTTCCTGCCAAA-3′ and 5′-CCGCTGCCATCTCTTCCT-3′). Amplification was made following a 30-s denaturation step at 98°C, as follows: 4 cycles of 98°C for 10 s, 60°C for 4 min, and 68°C for 5 min; 34 cycles of 98°C for 5 s, 60°C for 2 min, and 68°C for 5 min; and a final incubation at 68°C for 10 min. In parallel with samples subjected to the whole procedure, additional aliquots of cells or of chromatin were processed to generate additional controls: without cross-linking (the entire procedure was performed with cells not incubated with formaldehyde) and without ligase (the entire procedure was performed, but no ligase was in the mix). These samples served to control the specificity of the ligation (opportunistic ligation by background proximity without cross-linking) and of the PCR (without ligase). The relative frequencies (*F*) of interactions detected by 3C were calculated as follows: $F = [1.9^{CT \text{ control region} - CT \text{ test region}}/\text{min}(E \text{ control region}; E \text{ test region})]/[1.9^{CT \text{ control region} - CT \text{ positive 3C control region}}/\text{min}(E \text{ control region}; E \text{ positive 3C control region})]$, where the amplification of control region (which was the same as that for the digestion controls) served to normalize the intersample variations in the amounts of DNA and the positive 3C control region is a genomic fragment that always ligated under any condition ligation of two adjacent. All values were normalized for their availability for ligation by taking into account the minimal (min) digestion efficiency measured for either extremity of the ligated product. As negative controls, we (i) tested the minus ligase samples for each interaction and (ii) assessed for interactions between the bait fragments of interest and two negative controls, which were a region within a GAPDH (glyceraldehyde-3-phosphate dehydrogenase) exon and one region of the cluster that was not identified as an interacting partner by our 4C screenings. We did not normalize the values obtained for test regions to those obtained for these negative controls, as they generally did not produce any amplification signal. However, whenever this had to occur, the interaction detected with the test region was not taken into account. The 4C interactions were considered to be only qualitative, due to the amplification step present in the procedure. Calculations made to determine interacting regions were the same as those for 3C, except that in this case, the amounts of DNA were sufficient to allow further normalization to the results for the negative controls. In this case, the $C_T$ value for the control region used was the lower one (maximum interaction) obtained in the whole set of ligation-produced fragments tested. We considered values which were at least 2-fold higher than those for the negative-control regions to be significant. Networks of long-distance chromatin interactions were generated with the Cytoscape application (41).

**qPCR and statistics.** All qPCRs used 1 μM specific oligonucleotides (Sigma; the sequences are provided in Table S1 in the supplemental material) and were performed on Bio-Rad MyiQ and Bio-Rad CFX96 machines using Bio-Rad iQ SYBR green Supermix with 50 rounds of amplification, followed by determination of melting curves. Primers for RT-PCR were designed using the QuantPrime design tool (http://www.quantprime.de/) (42). Oligonucleotides for all other types of samples were designed with the Primer3 program (http://frodo.wi.mit.edu/primer3/). Values for ChIP samples were normalized in three steps: to those of the inputs ($\Delta C_T$), then to those of control ChIP samples (beads alone or anti-H3 ChIP; $\Delta\Delta C_T$), and then to the $\Delta\Delta C_T$ values obtained for control DNA regions. FAIRE values were normalized to the value for a positive-control region (the promoter of the *Rplp0* gene). All heat maps for qPCR data were generated with the Mev program (43), and values were determined to be significantly different from those for the control by the Wilcoxon or Student *t* test (depending upon the number of values). To facilitate their reading, only values significantly different from the control ones were included within the heat maps.

**Microarray data accession numbers.** Data set were deposited in the NCBI Gene Expression Omnibus database (http://www.ncbi.nlm.nih.gov/geo/) (44) under accession numbers GSE23850 and GSE32132 for the expression and ChIP-chip data, respectively.

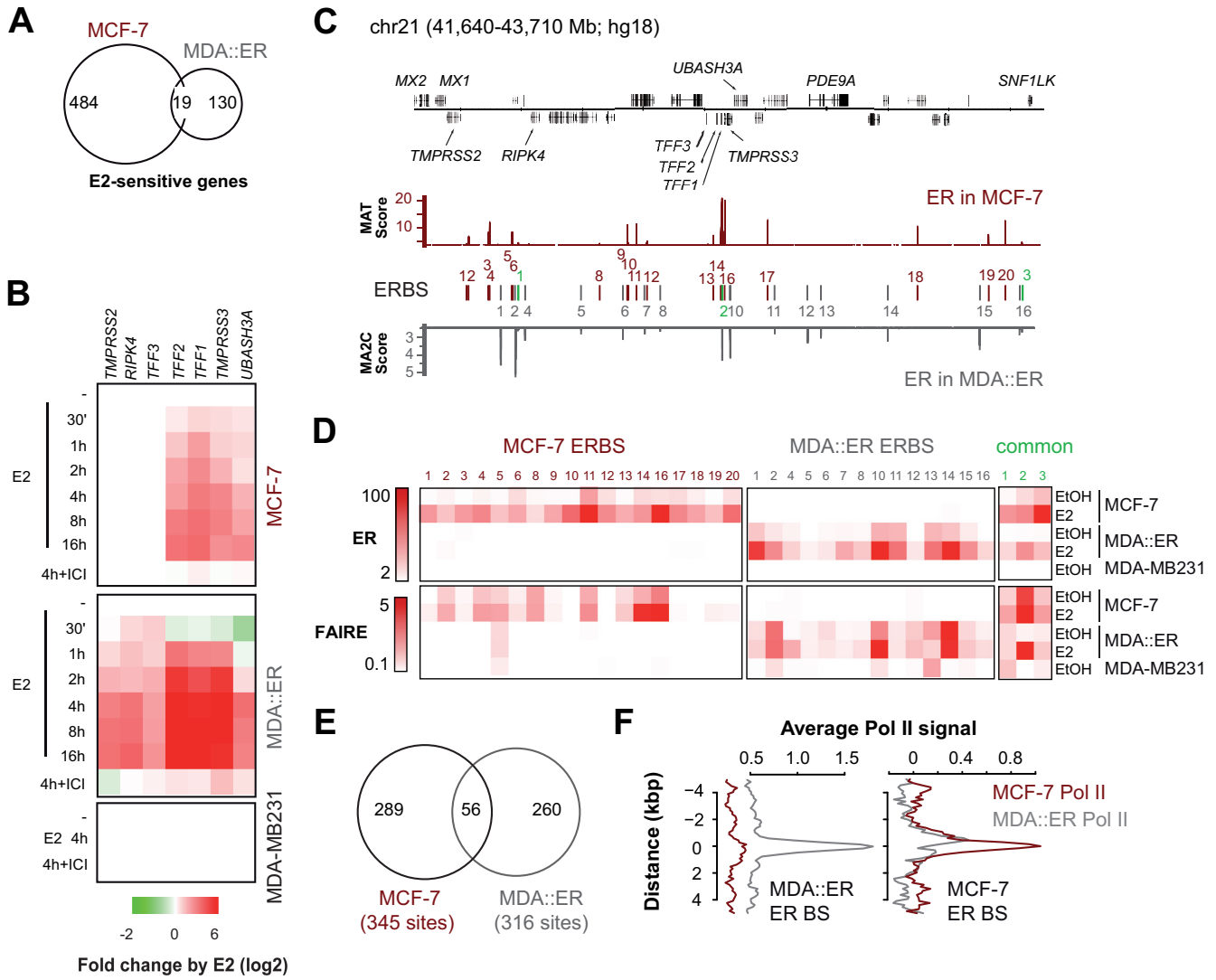


**FIG 1** Cell-specific E2-sensitive genes and ER binding sites in a 2-Mb genomic region, including the TFF locus. (A) Venn diagram illustrating the overlap of identified E2-sensitive genes in MDA::ER and MCF-7 cells. (B) Heat map representation of RT-qPCR results obtained with RNAs prepared from MCF-7, MDA::ER, and MDA-MB231 cells treated for the indicated times with $10^{-8}$ M E2 and pretreated for 36 h with $10^{-6}$ M ICI 164,384, where indicated. Results are the $\log_2$ values of the fold induction of gene expression by E2 obtained in two independent triplicate experiments. (C) Integrated Genome Browser (81) illustration of the studied genomic region with the RefSeq genes indicated. The ER binding signal obtained in an ER ChIP-chip analysis performed using the chromatin of MDA::ER cells treated for 50 min with E2 is depicted in gray. MCF-7 cell data were obtained from a published data set (17). For the sake of clarity, only the highest 5% of the signals are shown. Gray and red boxes, cell-specific ERBSs; green boxes, common ERBSs. (D) Anti-ER ChIP and FAIRE assays were conducted using chromatin prepared from MCF-7, MDA-MB231, or MDA::ER cells treated with E2 or ethanol (EtOH) as a vehicle control for 50 min. Results shown within heat maps are the means of 6 to 9 values obtained in independent triplicate experiments. Values are the fold enrichment over the value for control samples and a negative-control region (the promoter of the transcriptionally active *Rplp0* gene). (E) Overlap of MDA::ER cell-specific ERBSs with MCF-7 cell-specific ERBSs on regions spotted on the arrays. (F) Enrichment signals obtained in anti-RNA Pol II ChIP-chip experiments performed with MDA::ER cells treated for 50 min with E2 (data for MCF-7 cells are from reference 17) were aligned on MCF-7 or MDA::ER cell-specific ERBSs identified within the regions spotted on the arrays and located more than 10 kbp away from the transcription start site of any annotated gene.

## RESULTS

**Cell-specific transcriptional regulation of TFF cluster and ERBSs.** To consider processes governing the coregulation of colinear genes by E2, we first characterized the MDA::ER and MCF-7 cell repertoires of E2-sensitive genes by microarray analyses. As shown in the Venn diagram in Fig. 1A, the estrogen-sensitive transcriptome of both cell types was extremely divergent, with the two cell types having only 19 genes in common after 4 h of E2 treatment. This is consistent with the findings of previous studies (45–47). We next identified clusters of E2-regulated genes defined as regions comprising at least 3 regulated genes within a window of 7 genes. As a paradigm, we focused here on one cluster located within locus 21q22.3 that was previously identified in MCF-7 cells (48) and termed TFF (Fig. 1). This choice was guided by the fact that (i) this region includes the prototypical estrogen-responsive gene *TFF1* and (ii) our transcriptome analysis indicated that this E2-sensitive region includes different E2-sensitive genes in MCF-7 and MDA::ER cells, with only 4 genes being regulated by

E2 in MCF-7 cells and up to 7 genes being regulated by E2 in MDA::ER cells. This indicated that specific events may influence the transcriptional response of genes included in this genomic region and thereby provided the opportunity to address these mechanisms. Note that we included the *TMPRSS2* gene in our definition of the estrogen-responsive TFF cluster, since it was found to be regulated by E2 in MDA::ER cells. We first performed RT-qPCR experiments to confirm this regulation. The results of these assays, illustrated in Fig. 1B, showed (i) a timely coordinated regulation of the expected genes by E2 and (ii) that ER is the main transcription factor responsible for their E2 responsiveness, since a 24-h pretreatment of the cells with the ER-targeting antiestrogen ICI 164,384 (ICI) abrogated the actions of E2 (Fig. 1B). Moreover, none of the tested genes were regulated in naive MDA-MB231 cells (Fig. 1B), further confirming that the observed gene regulation by E2 strictly relied on the presence of ER.

These different subsets of estrogen-sensitive genes between MCF-7 and MDA::ER cells might reflect the existence of different ER cistromes in the two cell lines. Hence, we characterized ER binding sites in this genomic region in MDA::ER cells. ER chromatin immunoprecipitation (ChIP) experiments were performed with chromatin prepared from MDA::ER cells treated for 50 min with $10^{-8}$ M E2, with the resulting samples being hybridized on custom tiling DNA arrays designed to cover genomic regions containing E2-sensitive clusters (Table 2). These assays identified 17 ERBSs within the TFF cluster in MDA::ER cells at an FDR of $<5\%$ (Fig. 1C). When these data were compared to the ERBSs determined in MCF-7 cells by use of the ChIP-chip technology (data from Carroll et al. [17]), only three binding sites were common to both cell lines (shown in green in Fig. 1C), including comBS2 located within the *TFF1* promoter. This low overlap between MDA::ER and MCF-7 cell-specific ERBSs is consistent with the findings of analyses performed with the entire genomic regions spotted on the arrays (Fig. 1D).

Independent anti-ER ChIP-qPCR assays confirmed the cell specificity of these ERBSs. Formaldehyde-assisted isolation of regulatory element (FAIRE) experiments further showed that MDA::ER cell-specific ERBSs exhibited a condensed chromatin state in MCF-7 cells and vice versa (Fig. 1E). This observation was also made when evaluating the enrichment of these regions in canonical histone marks for enhancers (not shown). Thus, the chromatin condensation state of these genomic sequences confirmed their cell-specific function. An exception to this observation was made for the MCF-7 cell-specific ERBS5, which also exhibited an open conformation in MDA::ER and MDA-MB231 cells. This might illustrate the vicinity of this sequence with an annotated transcript. Recent data have shown that transcription can occur at enhancers (49–51). This prompted us to assess by ChIP-chip whether RNA polymerase II (Pol II) was present on MDA::ER cell-specific ERBSs. As shown in Fig. 1F, we indeed found a general enrichment of MDA::ER cell-specific ERBSs in Pol II that further exhibited cell specificity since it was not observed in sequences corresponding to MCF7 cell-specific ERBSs. Concordantly, the use of previously published MCF7 cell Pol II ChIP-chip data (17) in these analyses also showed that the polymerase was enriched on MCF7 cell-specific ERBSs but not MDA::ER cell-specific ERBS sequences (Fig. 1F).

In conclusion, these results altogether show that the studied 2-Mb genomic region that covers the TFF cluster includes different sets of estrogen-responsive genes and ERBSs in MCF-7 and MDA::ER cells. Interestingly, the cell-specific ERBSs were not predominantly found in the proximity of cell-specific E2-regulated genes. In accordance with the fact that chromatin loops may place the promoter of these cell-specific genes in the vicinity of cell-specific ERBSs (15), the latter observation suggested that the three-dimensional organization of the TFF loci may differ between the two cell lines.

**Dynamic spatial reorganization of the TFF cluster upon E2 treatment.** We next envisioned that the coordinated regulation occurring at the level of the studied genomic region in both MCF-7 and MDA::ER cells (Fig. 1) may involve an E2-dependent spatial reorganization of this locus. To test this hypothesis, we performed DNA-FISH experiments. A noteworthy finding was that MDA::ER cells presented three fluorescent TFF loci, and there were a higher number of loci (at least six) in our MCF-7 cell line. This originates from the complex hypertriploid karyotype of these MCF-7 cells, which harbor 3 chromosomes 21 and multiple nonassignable chromosome parts that contain at least four TFF loci (see Fig. S1 in the supplemental material). As this high number of loci hindered the correct evaluation of the experimental results, we focused on MDA::ER cells for these specific analyses. We first conducted experiments aiming to evaluate the spatial volume occupied by the 2-Mb genomic region encompassing the TFF cluster and thus performed DNA-FISH with a mix of fluorescent probes generated from multiple BACs covering a large part of the TFF region (Fig. 2A). The results of these experiments led us to evidence a compaction of the chromatin domain containing the TFF cluster after a 50-min treatment with E2 (Fig. 2B). This could be assigned to a smaller dispersion of the distances separating the central (B5) and 5′ (B1) probes following exposure to E2 (Fig. 2C). Interestingly, while there were no changes in the distribution of distances between probes generated using the central and the 3′ (B6) BACs, the distribution of the distances separating probes located at both extremities of the TFF region was again significantly different. Furthermore, quantile-quantile representations (Q-Q plots) of the data (Fig. 2C, bottom) indicated that the observed changes mostly reflected the disappearance of large distances separating paired probes. Importantly, these variations were not an indirect consequence of a global reduction in the volume of the nucleus upon E2 exposure (not shown). The 2-Mb region containing the TFF cluster thus undergoes spatial rearrangements under E2 treatment in MDA::ER cells, reflected by a more constrained three-dimensional conformation.

To gain further insight into how the cell-specific transcriptional activity of the TFF cluster was spatially organized, we characterized the spatial proximity of the ERBS with the promoters of E2-regulated genes. We conducted 4C-qPCR on chromatin prepared from MCF-7, MDA::ER, as well as MDA-MB231 cells all treated for 50 min with E2. The results of these experiments (see Fig. S2 and S3 in the supplemental material) are shown schematically in Fig. 3A. All determined spatial proximities are given in Table S2 in the supplemental material. These 4C assays recovered all but one of the interactions previously determined by chromatin interaction analysis by paired-end tag sequencing (ChIA-PET) (15) to link ERBSs to regulated promoters in MCF-7 cells and further uncovered 38 new interactions (Fig. 3B), in agreement with the differing outcomes of the 4C and ChIA-PET techniques. These experiments indicated that major spatial constraints of this chromatin domain involve interactions between central and distant regions mainly located 5′ of the TFF cluster (approximately

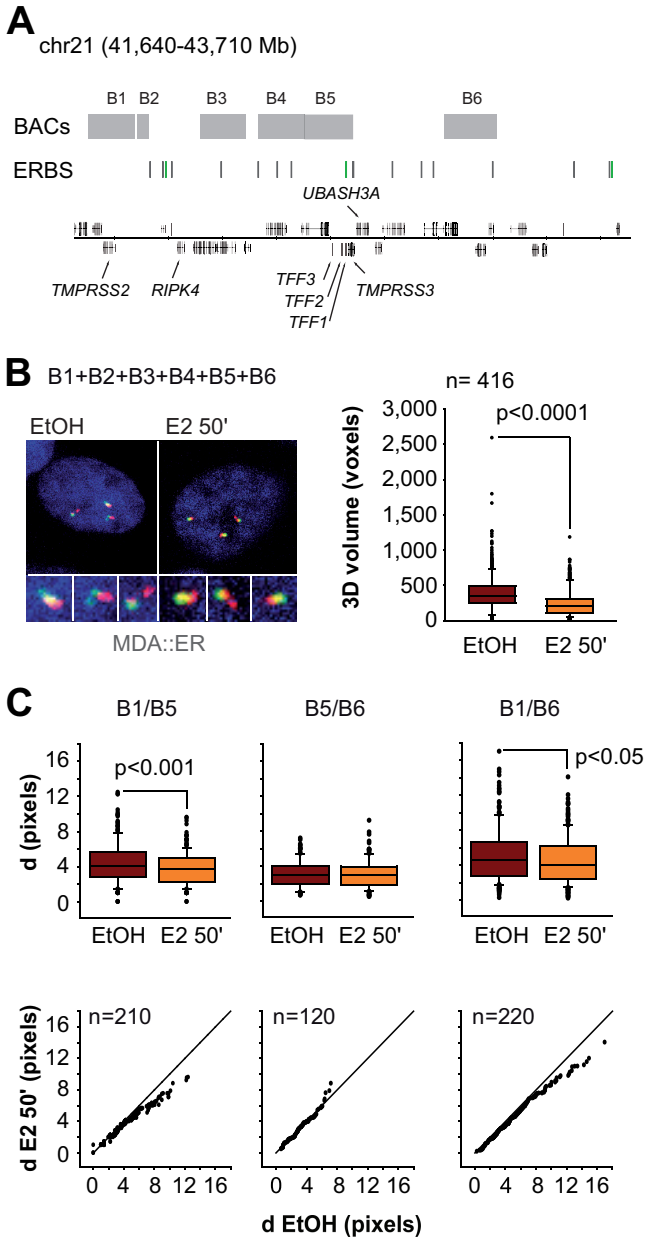


**FIG 2** E2 provokes a three-dimensional reorganization of the TFF cluster in MDA::ER cells. (A) Locations of the BACs (B1 to B6, referring, respectively, to RP11-814F13, CTD-2337B13, RP11-35C4, CTD-260o11, RP11-113F1, and CTD-1033M14) used to generate fluorescent probes for FISH experiments all along the genomic region of interest, as illustrated in Fig. 1. The positions of the ERBSs are also indicated. (B) Analysis of the 3D volume of the TFF loci by DNA-FISH using a mix of all generated probes in cells treated with $10^{-8}$ M E2 or ethanol (EtOH) for 50 min. (Left) Representative pictures of the results of these assays, with magnified views of the three TFF loci present in MDA:ER cells given below; (right) quantitative measurements ($n = 416$) of the 3D volumes of the loci, with the *P* value obtained by the Fisher *t* test indicated. (C) Quantitative analysis of the distribution of distances separating the indicated paired FISH probes. Values are shown within box plots (top) or within quantile-quantile (Q-Q) plots representing conditionally ranked measured distances (bottom). The normal distribution expected from nonvariant distances is illustrated by the straight line in each Q-Q plot. *P* values obtained by a nonparametric Fisher test are indicated when they were determined to be significant, as are the number of measurements made in at least three independent experiments. d, distance.

70% of the ERBS-promoter interactions) in both MCF-7 and MDA::ER cells. This is consistent with results obtained in DNA-FISH experiments. Interestingly, the *RIPK4* promoter was situated in the spatial vicinity of more ERBSs in MDA::ER cells than in MCF-7 cells (Fig. 3A and C). This might be correlated with the estrogenic regulation of this gene in the former cell line but not in the latter (Fig. 1). However, there was no strict correlation between the numbers of ERBS-promoter interactions and the amplitude of the estrogenic regulation of the gene, as evaluated by the RT-qPCR results from Fig. 1 (maximum $R^2$ values of 0.22 and 0.51 were observed following 2 h of E2 treatment for MCF-7 and MDA::ER cells, respectively). Importantly, 27% of the interactions detected in MDA::ER cells were also detected in ER-negative MDA-MB231 cells. This indicates that some of the MDA::ER cell-specific ERBSs may be preexisting enhancers that recruit additional transcription factors regulating the activity of all considered genes, with the exception of *TFF3*, as it did not establish any contact with the tested regions in MDA-MB231 cells (Fig. 3A and C). Conversely, since the remaining 73% of the interactions detected in MDA::ER cells were not detected in MDA-MB231 cells, these results also demonstrate that the expression of ER in this system is sufficient, either directly or not, for remodeling of the spatial organization of this genomic region.

As illustrated in Fig. 3D and E, the network of interactions between ERBSs and promoters of regulated genes in MCF-7 and MDA::ER cells is complex. One striking difference between these interactomes detected by 4C is that there are more singleton interactions in MCF-7 cells than in MDA::ER cells. Indeed, while six ERBSs were interacting with a single gene in MCF-7 cells, there was only one of these exclusive contacts in MDA::ER cells (the BS15/*TFF3* association). Finally, this interactome study also showed that the ERBS located within the *TFF1* promoter (comBS2) directs more interactions than the others in both cell lines, suggesting that it plays a crucial role in the chromatin reorganization of the TFF cluster in response to E2.

**CTCF and cohesin are required for appropriate regulation and organization of the TFF cluster.** ER has been proven to modulate the frequencies of interactions between distant ERBSs and the promoters of either up- or downregulated genes (15, 52), in concert with CTCF and/or the cohesin complex (53). Hence, to better understand how E2 signaling impacts chromatin organization, we mapped CTCF and RAD21 (a subunit of the cohesin complex) binding sites in MDA::ER cells through ChIP-chip analysis (Fig. 4A). The comparison of all the MDA::ER CTCF BSs and RAD21 BSs identified on all the genomic regions spotted on our arrays with those previously determined in MCF-7 cells (53) (restricted here to BSs contained within the spotted regions) indicated that most CTCF BSs were conserved between the two cell types, in contrast to the findings for RAD21 BSs (Fig. 4B). This cell-specific RAD21 cistrome may represent a major source for the different E2 responses of the clustered TFF genes. On the other hand, the overlap between the BSs for ER, CTCF, and RAD21 within the TFF cluster was much more important in MCF-7 cells than in MDA::ER cells (Fig. 4C). These different ER/CTCF/RAD21 BS overlaps between MCF-7 and MDA::ER cells were reflected in the proportions of established contacts between ERBSs and gene promoters (Fig. 4D). These data also indicate that the presence of CTCF and/or RAD21 at ERBSs does not correlate with the number of interactions made with gene promoters in the context of the TFF cluster (chi-square and Fisher tests, $P > 0.4$). In

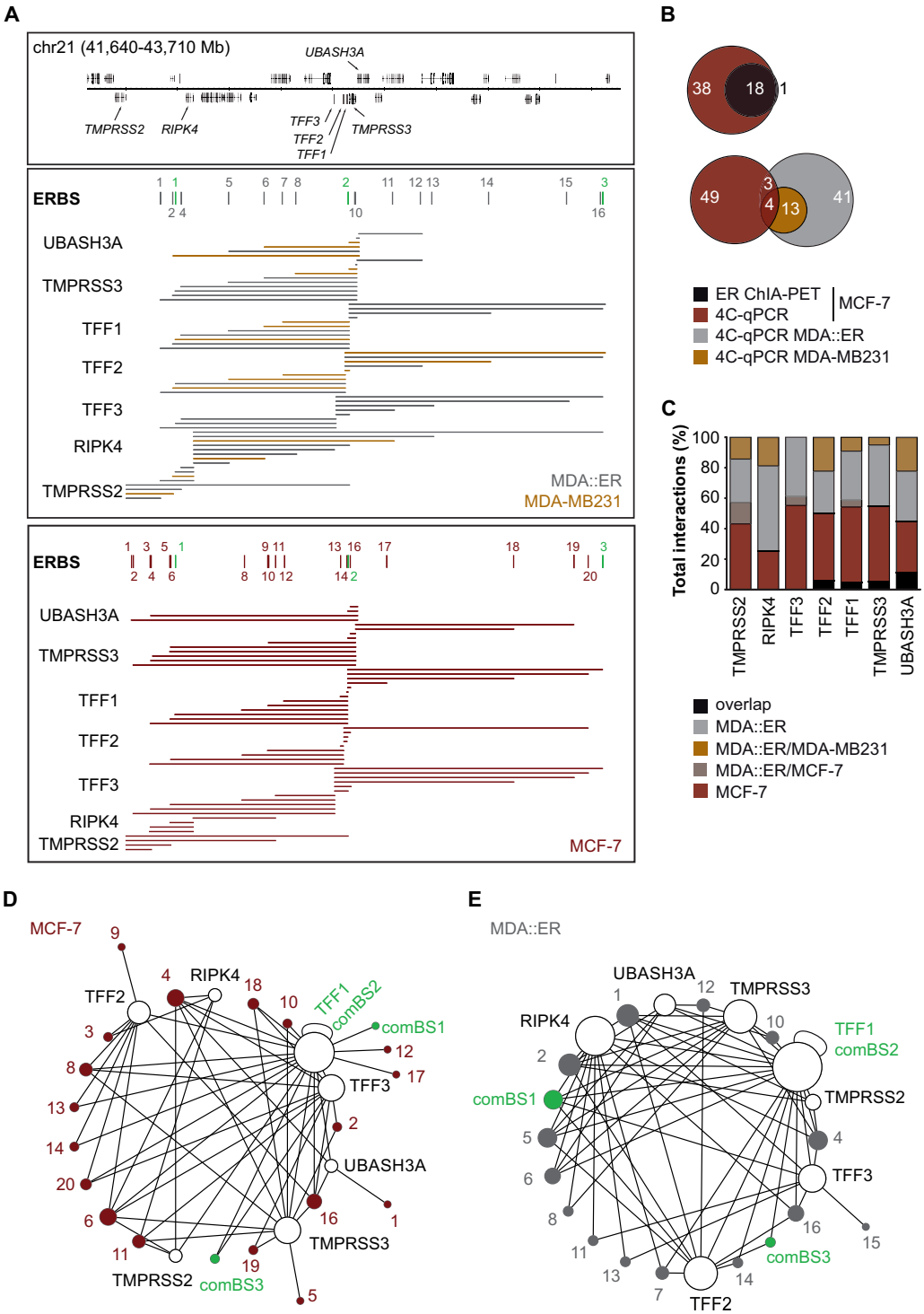


**FIG 3** ERBS-promoter interactomes. (A) Integrated Genome Browser visualization of MCF-7, MDA-MB231, and MDA::ER cell interactomes linking DpnII fragments encompassing ERBS or promoter regions of the indicated genes, as detected by 4C-qPCR on chromatin prepared from cells treated for 50 min with $10^{-8}$ M E2. Shown are RefSeq gene coordinates along chromosome 21 (chr21), as well as the positions of ERBSs. Gray, red, and green, MDA::ER cell-specific ERBSs, MCF-7 ER cell-specific ERBSs, and common ERBSs, respectively. 4C data are represented as lines linking one ERBS to its target promoter. Red, MCF-7 cell interactions; gray, MDA::ER cell interactions; orange, interactions shared between MDA::ER and MDA-MB231 cells. (B) Venn diagrams depicting the overlapping interactions characterized in this study and those identified in the published ER ChIA-PET data set (15) restricted to loops involving the gene promoters that served here as 4C bait. (C) Stacked histograms illustrating the overlap of the 4C-detected interactions for each tested promoter in the different cell lines. (D and E) Cytoscape (41) circular layouts of the networks of interactions that link E2-regulated genes to ERBSs in MCF-7 cells (D) and in MDA::ER cells (E). The sizes of the nodes are directly related to the number of interactions that they direct.

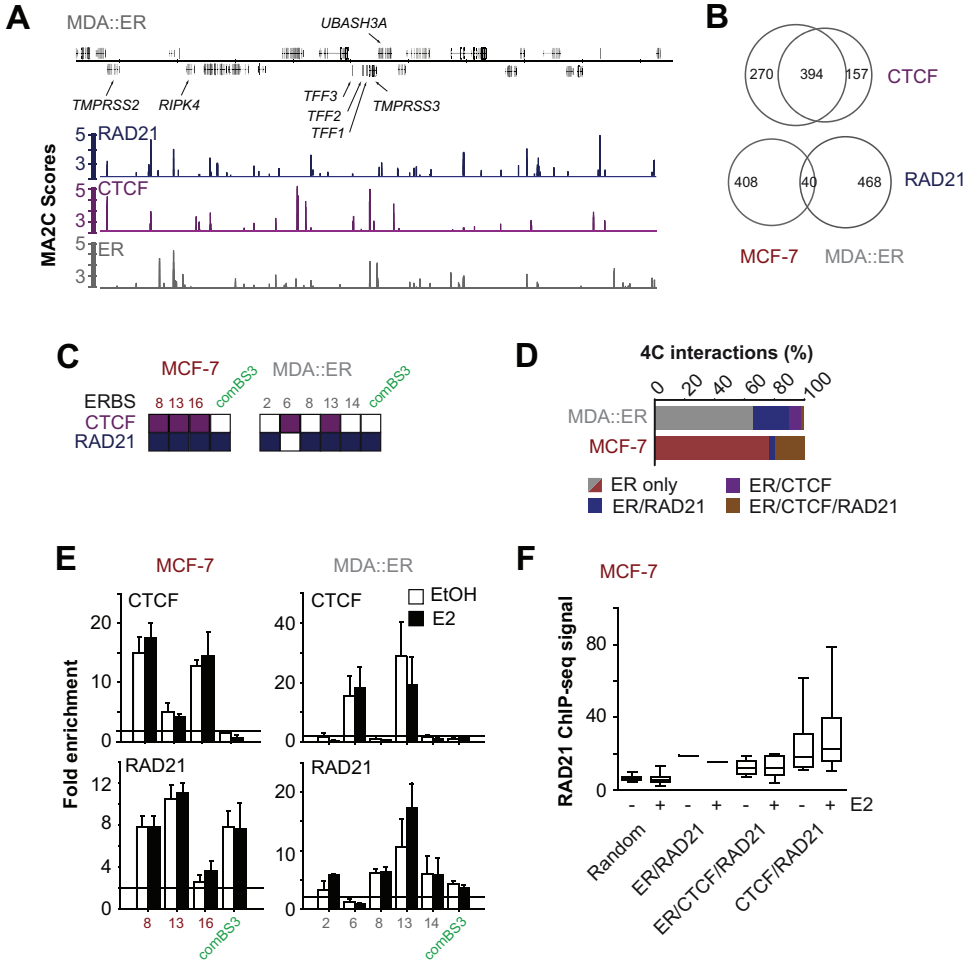


**FIG 4** CTCF and cohesin recruitment to ERBSs. (A) MDA::ER cell anti-ER, anti-CTCF, or anti-RAD21 ChIP-seq or ChIP-chip signals visualized under an Integrated Genome Browser, as described in the legend to Fig. 1. All data were obtained from cells treated with $10^{-8}$ M E2 for 50 min. (B) Overlap on array-spotted regions between RAD21 or CTCF binding sites determined in this study in MDA::ER cells and those previously determined in MCF-7 cells (53). (C) Overlap of RAD21 and CTCF binding sites with ERBSs. (D) Repartition of CTCF and RAD21 BSs within the interactions between ERBSs and gene promoters identified by 4C. (E) CTCF and RAD21 ChIP-qPCRs were performed on chromatin prepared from MCF-7 or MDA::ER cells treated for 4 h with $10^{-8}$ M E2 or ethanol (EtOH) as a vehicle control. The fold enrichment of the precipitated proteins for the tested sequences was normalized to the values obtained by control ChIP and for the negative region (*PKNOX1* promoter). Data shown are mean values ± SDs obtained in three independent triplicate experiments. The lines depict the significance threshold applied (fold enrichment, >2). (F) Box plots of the MACS-normalized reads of the RAD21 ChIP-seq experiments performed in the absence or presence of E2 in MCF-7 cells (the data are from reference 53). Values shown are the mean counts measured in a 500-bp window centered on the indicated binding sites located within the 2-Mb genome region studied. Calculations were also made for an equal number of random sites with a mean size similar to that for the shared CTCF/RAD21 BSs and equal in number to that for the shared CTCF/RAD21 BSs.

agreement with this observation, we did not observe any significant increase in CTCF and RAD21 binding to the respective ERBSs following the addition of E2 (Fig. 4E). This may signify that the dynamic modulation of the TFF three-dimensional organization that occurs upon E2 treatment involves other RAD21/CTCF sites. Alternatively, the physical contacts established between the ERBSs and the promoters may be directed by ER and occurring within a structurally fixed frame imposed by CTCF and/or RAD21. In favor of the latter hypothesis, the alignment of RAD21 ChIP-seq reads obtained in MCF-7 cells (data from reference 53) on ER, CTCF, and RAD21 shared binding sites within the TFF cluster did not provide evidence of any significant change in RAD21 mobilization on ER/CTCF/RAD21 BSs, on the sole ER/RAD21 BS, or on CTCF/RAD21 BSs ($P = 0.0676$ for the last category of sites) (Fig. 4F).

The putative role of CTCF and RAD21 in establishing the spatial conformation of the TFF cluster genomic domain was next examined following the transfection of siRNAs targeting their expression. The results of control RT-qPCR and Western blotting assays performed with MDA::ER cells are shown in Fig. 5A and B, and similar results (reductions) were observed in MCF-7 cells (not shown). We first performed 3C-qPCR experiments to evaluate the impact of these siRNA-mediated reductions in CTCF and RAD21 intracellular amounts on the frequencies of interaction between RAD21- and/or CTCF-positive ERBSs and the promoters of E2-regulated genes. These experiments, whose results are summarized in Fig. 5C, showed that the silencing of RAD21 diminished the frequency of interactions between ERBSs and their target gene promoters in both MDA::ER and MCF-7 cells. This was also observed following the transfection of siRNAs targeting CTCF

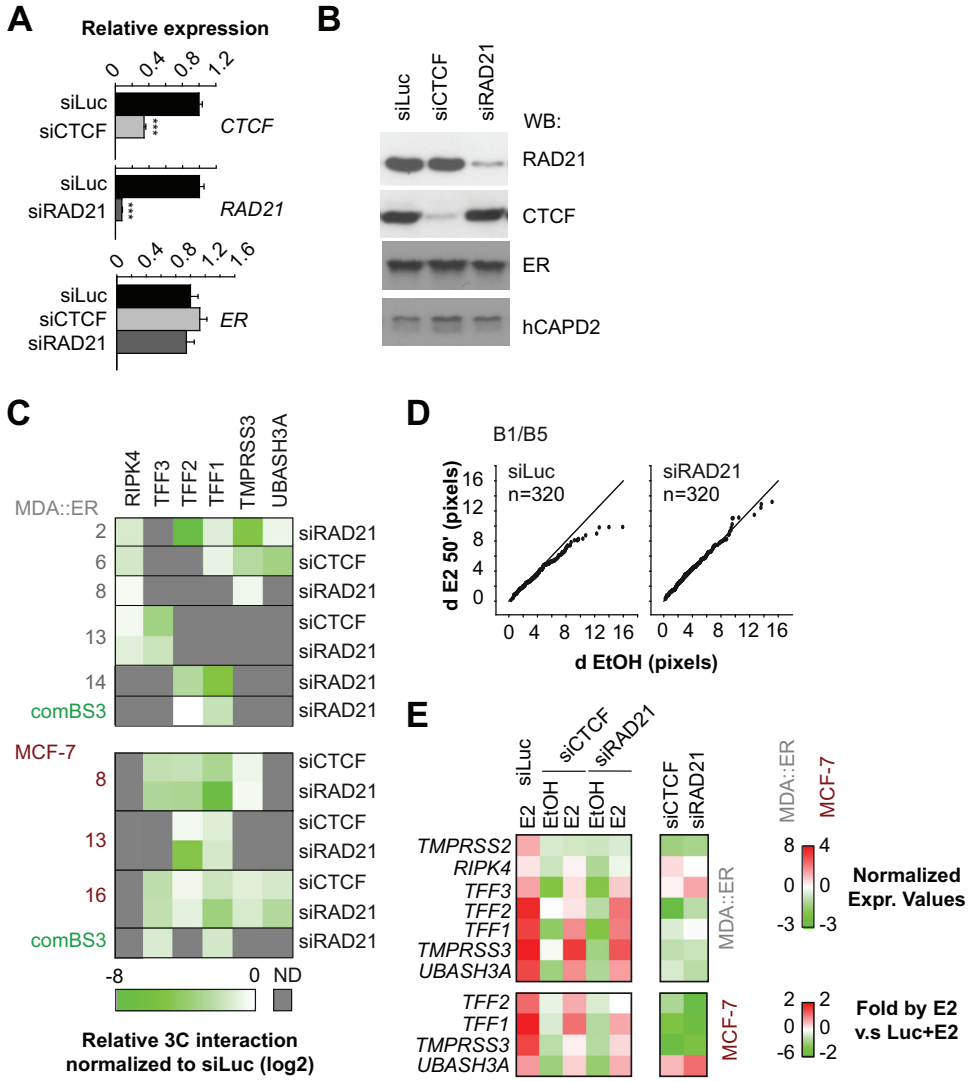


**FIG 5** CTCF and cohesin organize the E2 responsiveness of the TFF cluster. (A) The amounts of the indicated mRNA were evaluated in untreated MDA::ER cells following 72 h of transfection with either control siRNA (siRNA directed against the luciferase gene [siLuc]) or siRNAs targeting mRNAs of interest. The results shown are mean data ± SEMs of values obtained in at least 5 different experiments (*n* range, 15 to 18) normalized to the level of expression of the control *PKNOX1* gene. The Wilcoxon test was used to identify statistically relevant variations from the control condition with siRNA directed against the luciferase gene and ethanol. ***, $P < 0.001$; **, $< 0.01$. (B) Western blots (WBs) assaying the expression of RAD21, CTCF, ER, and hCAPD2 (loading control) in cells transfected with the indicated siRNAs. (C) 3C-qPCR experiments following the impact of the reduction in CTCF and RAD21 contents on the interactions between the indicated ERBSs and gene promoters. The results shown originated from one representative experiment out of two and are expressed as the $\log_2$ values of the values normalized to those obtained under the control condition with siRNA directed against the luciferase gene. (D) Quantitative DNA-FISH analysis of the distribution of distances separating paired fluorescent probes in transfected MDA::ER cells. Results are illustrated as described in the legend to Fig. 3. (E) Heat maps summarizing the RT-qPCR results obtained in at least 3 independent triplicate experiments following the transfection of control siRNA directed against the luciferase gene or siRNAs directed against CTCF or RAD21 expression and 4 h of treatment of the cells with $10^{-8}$ M E2 or ethanol as a vehicle control. (Left) Expression (Expr.) levels were normalized to the level for the *PKNOX1* internal control and are reported relative to those calculated for the condition with siRNA directed against the luciferase gene and ethanol. (Middle) Fold induction of gene expression by E2 relative to that measured for cells transfected by the siRNA directed against the luciferase gene. Results originate from at least four independent triplicate experiments.

(siCTCF), although to a lesser extent (Fig. 5C). DNA-FISH experiments further showed that RAD21 is essential for the global E2-induced constraints exerted on the TFF three-dimensional conformation (Fig. 5D). Unfortunately, the involvement of CTCF could not be addressed here due to its inefficient depletion (≈25%) in this particular experimental setup. Finally, disrupting CTCF and RAD21 expression by siRNAs drastically reduced both the basal and induced transcriptional activity of E2-regulated genes in both cell lines (Fig. 5E). This ultimately led to a strong decrease of the fold inductions by E2 for all genes except *TFF3* and *RIPK4* in MDA::ER cells and *UBASH3A* in MCF-7 cells.

Altogether, these data indicate that cohesin and CTCF organize the E2 responsiveness of the genes included in the TFF cluster in both cell lines, possibly by promoting a three-dimensional organization of the studied genomic locus which is propitious for the interaction between distant ERBSs and promoters of activated genes.

**Dynamic 3D organization of the TFF cluster.** We next ques-

tioned whether one or a limited number of ERBSs within the TFF cluster could orchestrate the observed coordinated gene regulation through long-range interactions. This hypothesis would imply that one or a few ERBSs are brought near promoters in a dynamic manner compatible with these transcriptional responses to E2. Hence, we evaluated by 3C-qPCR the dynamics of the interactions between ERBSs and gene promoters following treatment of the cells with E2. Data obtained with MCF-7 or MDA::ER cells are summarized in Fig. 6 and Fig. 7, in which the sizes of the circles are directly proportional to the fold changes in the relative frequency of interactions compared to that in the initial situation (time zero) (data for MCF-7 cells are presented in Fig. S4 in the supplemental material). The *x* axes show the coordinates for the promoters of the genes, and the *y* axes show the coordinates for the ERBSs, whose positions are indicated. Importantly, all of the ERBS-promoter interactions were detected at time zero (data for the MCF-7 cell controls are presented in Fig. S4 in the supplemental material). In both cell types, a spatial reorganization was apparent as soon as 10 min following E2 addition, with both increases and decreases in the frequencies of interaction being detected (Fig. 6 and 7). The existence of several TFF loci in both cell types may influence the interpretation of these kinetic 3C data, since we could not ascertain that all of the interactions were occurring on the same genomic fragment. However, supporting the existence of dynamic variations in the three-dimensional organization of the TFF genomic region, we were able to further evidence such processes by DNA-FISH time course experiments in MDA::ER cells (see Fig. S5 in the supplemental material). Some of the reorganizations evidenced by 3C-qPCR exhibited a relatively dynamic or even cyclical nature, such as those highlighted in orange in Fig. 6 and 7. Interestingly, the dynamics of these spatial reorganizations differed between MDA::ER and MCF-7 cells. In MCF-7 cells, these variations were restrained to short-range interactions, except for *TFF1*/BS1, *TFF1*/BS18, and *TMPRSS3*/BS8 contacts (Fig. 6). In contrast, the dynamic MDA::ER cell interactome highlighted important variations in long-range interactions between ERBSs and the promoters of regulated genes. This is notably illustrated by the interactions made by the ERBSs located in the 5′ region of the cluster that climaxed at 50 min following the addition of E2 (Fig. 7). Furthermore, in MDA::ER cells, an apparent combination of local interactions (BS2 and comBS1) and long-range interactions (comBS2 and even comBS3 located at the far 3′ end of the genomic region) could be correlated with the E2-mediated regulation of *TMPRSS2* and *RIPK4*. In contrast to what happens in MCF-7 cells, the regulation of core TFF genes would thus be more influenced by distal than by local ERBSs in MDA::ER cells. Indeed, variations of the interactions made between ERBSs located within the *TFF3* to *TMPRSS3* (core TFF cluster) region appeared to be less important than what was observed in the case of MCF-7 cells.

In conclusion, these data indicate that there is no single major ERBS that organizes the responsiveness of E2 within this genomic region. Keeping in mind that 3C-based assays have the intrinsic limitation of being unable to ascertain the co-occurrence of the interactions detected in the same cell, we propose that the coordination of the transcriptional response of the TFF cluster to E2 mainly originates from a combinatorial engagement of ERBSs located within the *TFF1* promoter in MCF-7 cells with two nearby ones (BS14 or BS16) and with those located in the distant 5′ region of the cluster in MDA::ER cells.

**E2 regulation of a given gene is driven by different ERBSs.** Although they are highly informative, the 3C data presented above did not allow us to establish the exact contribution of each ERBS to the specific regulation of the genes that it contacts. To investigate at the molecular level the contribution of a given ERBS in regulating specific genes, we used small triplex-forming oligonucleotides (TFOs) to interfere with ER binding at a given BS (Fig. 8A). Such oligonucleotides that form Hoogsteen or reverse Hoogsteen hydrogen bonds with the purine-rich strand of DNA have already been used to inhibit the transcription of genes such as *ets2* (54) and c-*myc* (55) (reviewed in references 56 and 57). We characterized 11 TFOs (Table 1) which were able (i) to form a DNA triplex *in vitro* (see the results for TFO anti-MCF-7 cell BS1 as an example in Fig. 8B; otherwise, see Fig. S6 in the supplemental material), (ii) to specifically bind to target sequences but not the *PKNOX1* promoter used here as a control (Fig. 8C; see Fig. S6 in the supplemental material), and (iii) to significantly disrupt ER binding to the corresponding ERBS (Fig. 8D; see Fig. S6 in the supplemental material). Although all of the designed TFOs did not precisely target the center of each ERBS defined here, as determined from the ChIP-chip profiles, we observed that their relative efficiency in disrupting ER binding was only mildly correlated to the distance separating the TFO target sequence from the center of the ERBS peak (Fig. 8E). The ability of TFOs to bind to their target sequence also seemed to be relatively independent of their chromatin status, as evaluated from their relative enrichment by FAIRE (Fig. 8F).

Subsequent RT-qPCR experiments showed that in the majority of tested cases, decreasing ER binding on one ERBS impacted the transcriptional status of the genes to which it was spatially close (Fig. 8G) but not that of control genes (see Fig. S7 in the supplemental material). However, the converse with no observable impact of ER binding disruption was also observed, for instance, the associations between the MCF-7 cell BS4 and *UBASH3A* and BS6 and *TMPRSS3* or the MDA::ER cell BS10 and *UBASH3A*. This seems to imply that the binding of ER to some distant sites might not be essential for the regulation of the analyzed genes. Alternatively, this could also indicate a functional redundancy between the enhancers controlling the activity of the tested E2-sensitive genes. The abrogation of ER binding to such sites would be compensated for by the activity of the others. Additionally, the reduced ER mobilization provoked by TFOs diminished the frequencies of interactions linking the targeted ERBSs with the promoters of their target genes (data not shown). Interestingly, these experiments also evidenced that decreased ER binding to some sites affected the transcriptional status of genes that they did not contact. This was observed, for instance, in MCF-7 cells for the effect of BS1 on *TFF3*, comBS1 on *TMPRSS2*, BS10 on *TFF2*, and BS14 on *TMPRSS2* and *TFF3*. This was also true in MDA::ER cells for the effect of BS10 on *RIPK4* and BS12 on *TMPRSS2*, *RIPK4*, and *TFF3*. As shown by Fullwood et al. (15) in ChIA-PET assays, the three-dimensional organization of chromatin can place distant ERBSs in the spatial vicinity. We therefore evaluated whether targeting the recruitment of ER on one ERBS by a specific TFO could reduce its mobilization on another ERBS (see Fig. S8 in the supplemental material). Results from these experiments indicated that the observed transcriptional collateral effects were due—at least in part—to the establishment of additional interactions between ERBSs themselves. For instance, the reduction of *RIPK4* and *TFF3* expression by the TFO targeting

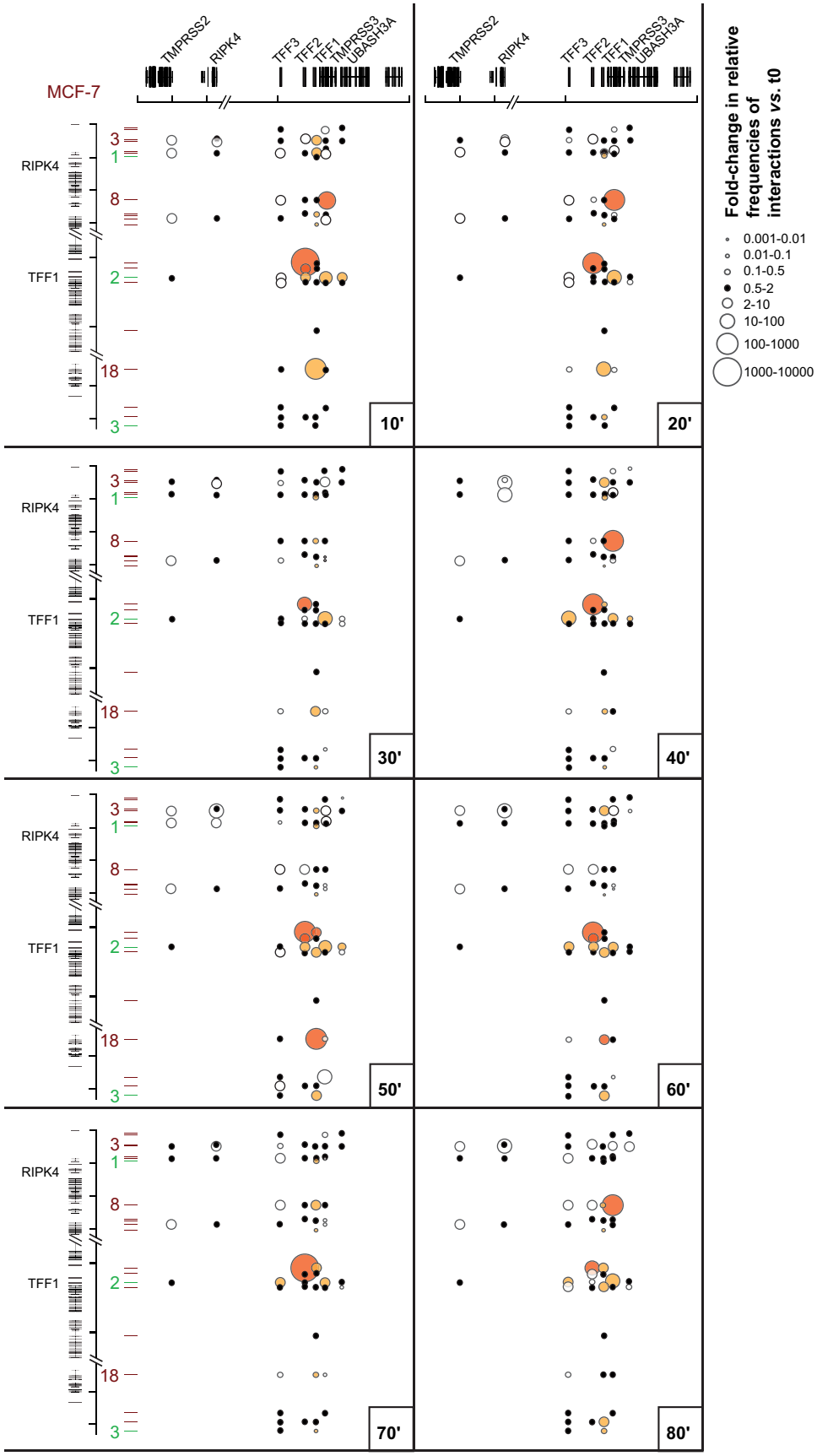

ERBS12 in MDA::ER cells could reflect a contact made between this ERBS12 and the ERBS16 that controls these genes.

The use of TFOs therefore allowed us to demonstrate the functional relevance of the interactions linking ERBSs to the E2-regulated promoters that we have characterized. Although they are limited to the ERBSs on which TFOs were able to disrupt ER recruitment, these data illustrate that the comERBS2 located in the close vicinity of the *TFF1* promoter plays a central regulating role in both cell types. They also clearly indicate that the MDA::ER cell ERBS1 and MCF-7 cell ERBS6 play prominent roles in the transcriptional activity of the genes included in the TFF locus.

## DISCUSSION

We investigated here the molecular processes allowing estradiol to coregulate the transcriptional activity of genes clustered within a 2-Mb genomic region. Using a naturally E2-responsive breast cancer cell line (MCF-7) and a cellular system with a forced E2 sensitivity (MDA::ER), we interrogated whether these mechanisms could be triggered by ER on its own. Despite different chromatin contexts, ER was found to drive tight regulation of the TFF cluster in both cell types, relayed by its mobilization on distinct genomic regions. Interestingly, the chromatin status of MDA::ER cell-specific ERBSs in native MDA-MB231 cells indicated that a number of ERBSs were already exhibiting an open conformation and characteristics of functional enhancers: enrichment in FAIRE experiments (Fig. 1), the presence of marks for poised or active chromatin (unpublished observations), and spatial proximity to the promoters of the considered genes (Fig. 3). Preparation of chromatin-to-ER binding in MCF-7 cells involves the actions of the pioneer factor FOXA1 (17, 58), which is not expressed in MDA::ER cells. Accordingly, all but four MCF-7 cell-specific ERBSs were FOXA1 positive. In contrast, ERBSs in MDA::ER cells were principally not located at sites bound by FOXA1 in MCF-7 cells, except for the common ERBSs ERBS2, ERBS3, and ERBS13. Hence, it may be that other factors act in a manner similar to that of FOXA1 in the MDA cell system or that ER acts on its own. Motif analysis performed on the entire set of MDA::ER cell-specific ERBSs identified in our ChIP-chip data indicated that, in addition to ERE motifs, GATA sites were also significantly enriched (not shown). This is consistent with reports showing that factors of this family, in particular, GATA3 (47, 59, 60), control ER activity.

4C and 3C assays allowed the description of dynamic interactomes linking ERBSs to promoters of genes. Some of the detected interactions, however, engaged promoters of genes that were not regulated by E2 in our RT-qPCR or transcriptomic data, such as *TMPRSS2*, *RIPK4*, or *TFF3* in MCF-7 cells. It is possible that these genes actually exhibit rapid transcriptional responses to estrogen like those evidenced by global run-on assays (GRO sequencing [49–51]), which we would have missed in our analyses for sensitivity and timeliness reasons. In contrast to what would have been expected from an artificial cellular model compared to what would have been expected from a more natural one, such as MCF-7 cells, we found that the ER-mediated three-dimensional reorganization of the TFF cluster response to E2 is more important and more intricate in MDA::ER cells. Indeed, there were more singleton interactions in MCF-7 cells, and the dynamic responses of the MCF-7 cell interactome following treatment with E2 were apparently lower than those in MDA::ER cells. It could be hypothesized that the chromatin three-dimensional structure of this whole genomic region is already prepared for a response to E2 in MCF-7 cells, in contrast to the reconstituted E2-sensitive cellular model provided by MDA::ER cells. If this is true, this implies that in MDA::ER cells, ER on its own is able to provoke important three-dimensional remodeling of the TFF locus to finely tune the transcription of target genes. Alternatively, the different levels of ploidy of our model cells (3 TFF loci in MDA::ER cells versus 6 in MCF-7 cells) may also impact the interpretation of the differences observed between the two cell types. For instance, the presence of inactive or E2-insensitive loci may hamper and reduce the variations observed in either cell line. Unfortunately, we were unable to ascertain by RNA-FISH that all loci were transcribed and regulated in these cells, presumably due to the small size of the TFF genes. However, E2-induced variations of the three-dimensional organization of the studied genomic region were observed in each of the 3 loci in MDA::ER cells. This suggests that all 3 loci may transcriptionally respond to E2 in this cell type.

The regulatory unit that integrates the TFF cluster is ~1 and ~2 Mb in size in MCF-7 and MDA::ER cells, respectively. These dimensions are consistent with those defined for topologically associating domains (TADs) from Hi-C and carbon copy circular chromosome conformation (5C) data (61–63). Hence, the different number of estrogen-sensitive genes between MDA::ER and MCF-7 cells could characterize the existence of cell-specific TAD geometries and different boundaries. CTCF and RAD21/cohesin have been proposed to delineate regions of correlated transcriptional regulation (64–66), even if their presence might not systematically reflect a demarcation between insulated gene domains (67). Our data extend observations made in MCF-7 cells regarding the involvement of CTCF and RAD21 in the establishment of key connections between distant ERBSs and regulated promoters of the TFF cluster (53, 68). We further showed that RAD21 is required for the proper folding of this genomic region and its response to estrogen. Studies in MCF-7 cells or mouse liver (53, 69) suggested that the main part of the action of RAD21 on tissue-specific expression or estrogenic regulation would be CTCF independent. Accordingly, the limited overlap of RAD21 binding sites in MCF-7 and MDA::ER cells indicates that the MDA::ER cell-specific cistrome of RAD21 engages cell-specific functions. Whether the cell-specific interactomes between ERBSs and gene promoters and the cell-specific size of the putative TFF TADs are directly linked to the different RAD21 cistromes between MCF-7 and MDA::ER cells remains an open question. One possible way to address this problem would be to define the chromatin loops es-

**FIG 6** Dynamic three-dimensional reorganization of the genomic region studied in MCF-7 cells. The results of one 3C experiment representative of two experiments performed with chromatin sampled from MCF-7 cells treated from 0 to 80 min with $10^{-8}$ M E2 are summarized. As indicated, the size of the circle that corresponds to one interaction is proportional to the fold change in the frequency of the interaction compared to that in the basal situation, i.e., that at time zero (t0). The locations of the gene promoters that served as anchors are illustrated at the top of each panel, and ERBSs are indicated on the left. The distance scale is accurate (2 Mb between tick marks) but had to be broken in some instances for the sake of figure size and clarity. Circles highlighted in orange are those commented on in the text, and those in yellow correspond to interactions made by the ERBS located within the *TFF1* promoter (comERBS2).

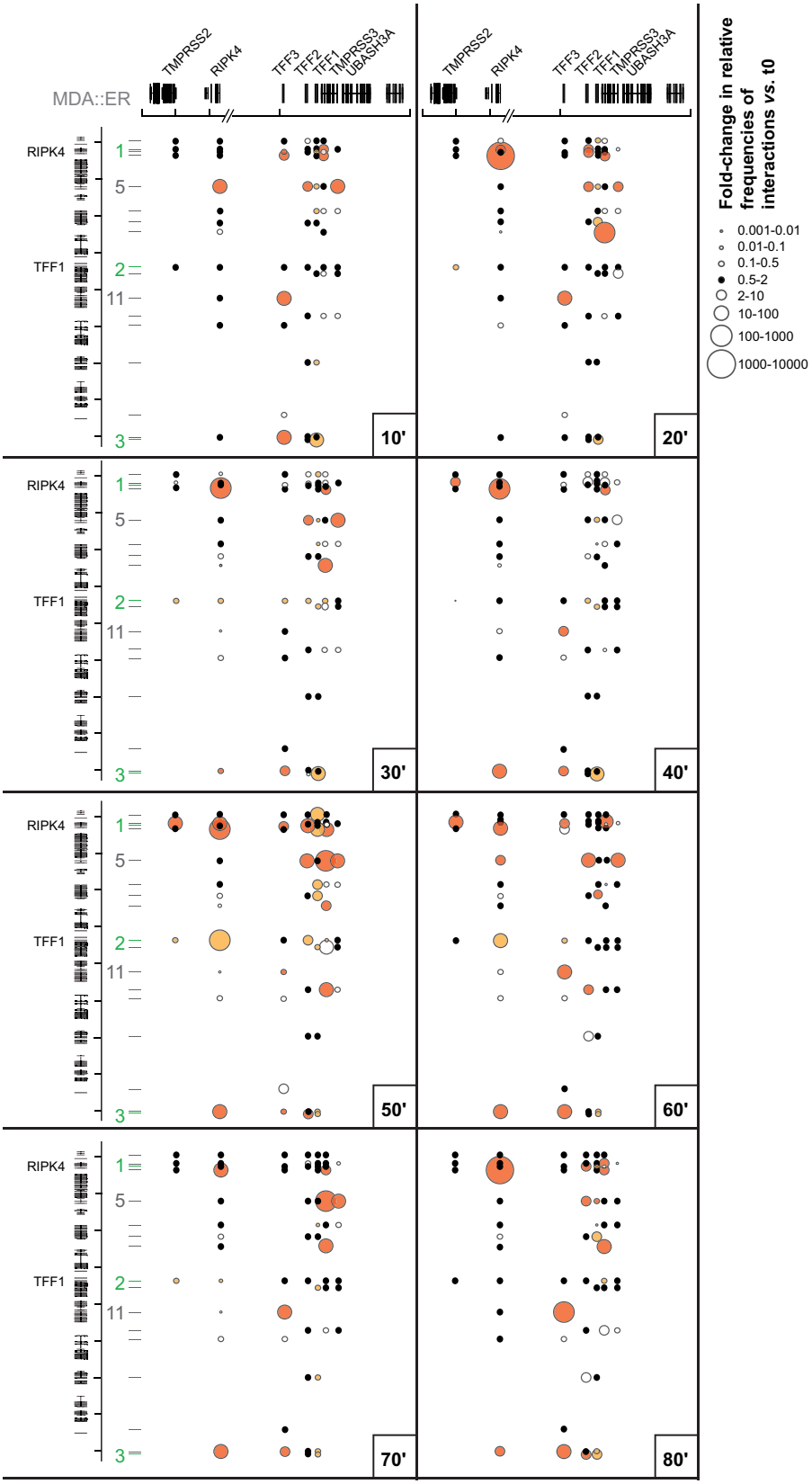


**FIG 7** Dynamic three-dimensional reorganization of the genomic region studied in MDA::ER cells. The results of one 3C experiment representative of two performed with chromatin sampled from MDA::ER cells treated from 0 to 80 min with $10^{-8}$ M E2 are summarized. See the legend to Fig. 6 for descriptions of the symbols.

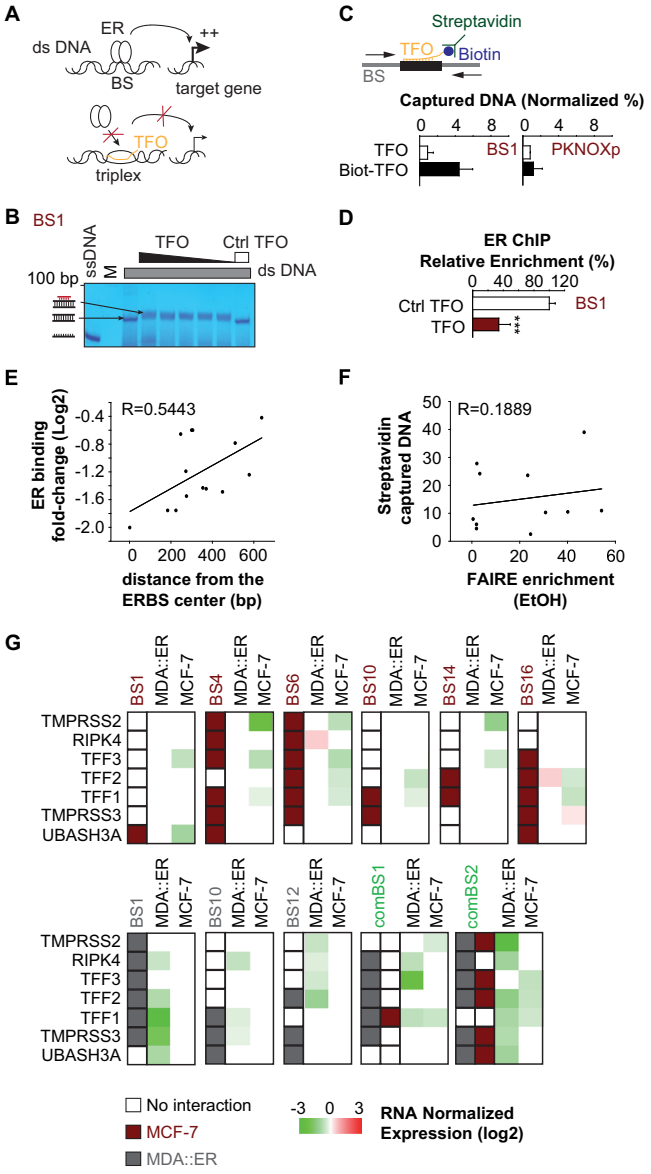


**FIG 8** Functionalization of MDA::ER and MCF-7 cell interactomes. (A) TFOs were designed to interfere with ER binding and, thus, to identify the roles of ER on specific BSs for the regulation of E2-sensitive genes. dsDNA, double-stranded DNA. (B) Formation of a DNA triplex analyzed by gel shift assay. Increasing amounts of TFO (25 to 1,500 pmol) were added to 25 pmol of target DNA duplexes, and the mixtures were incubated for 16 h at 37°C. A control was made using an unspecific TFO (Ctrl TFO) at the highest concentration. Complexes were separated by electrophoresis and stained with methylene blue. Lane ssDNA, single-stranded DNA; lane M, molecular mass markers. (C) MCF-7 cells were transfected for 36 h with 10 μmol of TFO or biotinylated TFO (Biot-TFO) directed against ERBS1 and subjected to cross-linking, and sonicated chromatin was then incubated with streptavidin-coated beads. The amounts of captured DNA were analyzed by qPCR. Values are means ± SDs of two independent duplicate experiments and are expressed as the percentage of captured DNA relative to the amount of input DNA normalized to the amount of the recovered negative-control region (*Rplp0* promoter). (D) Anti-ER ChIP-qPCR performed with MCF-7 cells transfected as described for panel C and treated for 50 min with $10^{-8}$ M E2. Results are mean values ± SDs of three independent triplicate experiments and are expressed as the level of enrichment relative to that for the *PKNOX1* promoter. (E) The fold change in ER mobilization measured by ChIP-qPCR of each tested ERBS following transfection of the corresponding TFO was plotted against the distance separating the sequence targeted by the TFO from the center of the ERBS defined from ChIP-chip data. (F) Amounts of streptavidin-captured DNA following the transfection of biotinylated TFOs are plotted against the relative chromatin accessibility of their target regions measured by FAIRE experiments under control conditions (ethanol [EtOH] vehicle control). (G) RT-qPCR experiments performed with MCF-7 and MDA::ER cells transfected with the indicated TFOs. The boxes at the left of each heat map indicate the interactions identified by 4C. Experimental values were normalized to those obtained with untransfected cells. Data originated from at least three independent duplicate experiments.

tablished between RAD21 BSs by ChIA-PET experiments in both cell lines.

In contrast to the slight increase reported at the genome scale by others (50, 51, 53), RAD21 recruitment to ERBSs in the TFF cluster was not significantly affected by E2. Whether this situation reflects an exception or a general behavior for clustered genes may constitute an interesting point to pursue in the analysis of the role of RAD21 in organizing chromatin domains. On the other hand, our observations are consistent with a model in which active chromatin compartments are organized through constitutive loci (64–66). The characterization of physical contacts between RAD21 BSs through ChIA-PET may help define the cohesin complexes that organize such compartments where dynamic contacts between enhancers and genes would occur (as proposed previously [70]). The nature of the mechanisms that underlie the E2-mediated remodeling of the TFF domain may therefore be directly or indirectly under the sole control of ER or of the estrogenic response of the genes. For instance, Mediator, a protein complex loaded on active promoters, can establish physical contacts between genes and promoters (71). In accordance with models of proximity ligation proposed by Gavrilov and coworkers (70), the recruitment of multiple proteins provoked by ER on its sites and its affinity with components of the transcriptional machinery would stabilize interactions that occur otherwise. It can also be inferred from this hypothesis that the mobilization dynamics of the proteins recruited by ER on chromatin (7, 8) may be at least partly responsible for the dynamic property of ERBS-promoter physical contacts. Such a process was evidenced in the case of the *CDKN1A* gene promoter placed under the transcriptional control of another nuclear receptor, the vitamin D3 receptor (VDR) (72). Accordingly, our kinetic 3C dissection of the three-dimensional reorganization of the TFF cluster indicates that all interactions between ERBSs and gene promoters already exist in the absence of E2. Hormone and ER binding would then have to be considered as signals that remodel preexisting conformations, a conclusion that seems to emerge from recent Hi-C data from a study which compared the global organization of MCF-7 cell chromatin in the absence of hormone and following 50 min of treatment (73).

A general problem that emerges from genome-wide studies is the evidence that the number of interactions made between the BSs of a transcription factor and genes promoters is not systematically reflected at the transcriptional level (74). The use of TFOs allowed us to provide further indications on how binding sites for a transcription factor are mobilized in space and time in order to regulate the transcription of its target genes. Although it has already been hypothesized (14, 17, 75), we demonstrate here the validity of the concept of functional redundancy between ER-bound enhancers. Indeed, a single promoter can establish contacts with several ERBSs, and we demonstrated that the resulting build out in some cases might be insensitive to inactivation of a partic-

ular ERBS, providing robustness to the regulatory system. In other cases, the mobilization of ER on distinct master regulatory regions appears to be sufficient to provoke the transcriptional response of the gene. Comparing the enrichment of main versus secondary ERBSs in particular histone modifications or ER, Pol II, CTCF, or RAD21 proteins or even their relative frequencies of interaction with their target promoters did not provide evidence of a particular segregating characteristic. The differential recruitment of the FOXA1, PBX1, and GATA proteins or yet uncharacterized cofactors may account for the specific use of a given ERBS or the collaborative use of several ERBSs. Alternatively, the existence of a particular master regulatory region may originate from a coincident propitious folding of local chromatin due to high-order organization and the presence of cognate DNA sequences mobilizing ER. Finally, our dynamic 3C experimental data taken together with results obtained following the transfection of TFOs also indicate that the role of one redundant enhancer toward that of another one may depend or shift over time or under different experimental conditions. The latter was suggested, for instance, from data comparing the recruitment of ER when activated by epidermal growth factor and E2 (76).

Although limited by the target sequence requirements, the nucleic acid composition of 2 to 7% of the ERBSs identified by ChIP-seq appears to be compatible with the binding of TFOs. Extending the experimental work flow used in this study to this whole subpopulation of ERBSs would give rise to a functionalized partial interactome that could greatly enhance our knowledge of the links existing between the functions of enhancers and the organization of the genome. Furthermore, as for ER, BSs for many transcription factors have been shown to be grouped around responsive genes in clusters of enhancers (77). Hence, TFOs or modified TFOs with increased efficiencies, such as peptide nucleic acids (PNAs) (78), locked nucleic acids (LNAs) (79), or bis-LNAs (80), may constitute powerful molecular tools to assess the generality of enhancer redundancy.

## ACKNOWLEDGMENTS

This work was supported by the CNRS and the University of Rennes I and benefited from grants from the ARC, the Ligue contre le Cancer (Equipe Labelisée Ligue 2009), the Région Bretagne (CREATE 4793), and the Agence Nationale pour la Recherche (ANR-09-BLAN-0268-01). S.H. was supported by funds from the Agence Nationale de la Recherche (JCJC-SVSE2-2011, ChromaTranscript project) and the European Union (FP7-PEOPLE-2011-CIG, ChromaTranscript project). J.Q. was the recipient of a joint fellowship from the CNRS and the Region Bretagne. A.A.S. was supported by a fellowship from the French Ministère de l'Enseignement Supérieur et de la Recherche, and S.C. was funded by a CNRS postdoctoral fellowship.

We greatly acknowledge Denis Habauzit for all his advice and help on the design and analysis of TFOs. We also thank Stephanie Dutertre and the other members of the Microscopy Rennes Imaging Center from the IFR biosit for technical assistance with the microscopes.

## REFERENCES

1. **Harmston N, Lenhard B.** 2013. Chromatin and epigenetic features of long-range gene regulation. Nucleic Acids Res. **41:**7185–7199. http://dx.doi.org/10.1093/nar/gkt499.
2. **Razin SV, Gavrilov AA, Ioudinkova ES, Iarovaia OV.** 2013. Communication of genome regulatory elements in a folded chromosome. FEBS Lett. **587:**1840–1847. http://dx.doi.org/10.1016/j.febslet.2013.04.027.
3. **Wei Z, Huang D, Gao F, Chang WH, An W, Coetzee GA, Wang K, Lu W.** 2013. Biological implications and regulatory mechanisms of long-range chromosomal interactions. J. Biol. Chem. **288:**22369–22377. http://dx.doi.org/10.1074/jbc.R113.485292.
4. **Cavalli G, Misteli T.** 2013. Functional implications of genome topology. Nat. Struct. Mol. Biol. **20:**290–299. http://dx.doi.org/10.1038/nsmb.2474.
5. **Van Bortle K, Corces VG.** 2013. The role of chromatin insulators in nuclear architecture and genome function. Curr. Opin. Genet. Dev. **23:**212–218. http://dx.doi.org/10.1016/j.gde.2012.11.003.
6. **McEwan IJ.** 2009. Nuclear receptors: one big family. Methods Mol. Biol. **505:**3–18. http://dx.doi.org/10.1007/978-1-60327-575-0_1.
7. **Métivier R, Penot G, Hubner MR, Reid G, Brand H, Kos M, Gannon F.** 2003. Estrogen receptor-alpha directs ordered, cyclical, and combinatorial recruitment of cofactors on a natural target promoter. Cell **115:**751–763. http://dx.doi.org/10.1016/S0092-8674(03)00934-6.
8. **Shang Y, Hu X, DiRenzo J, Lazar MA, Brown M.** 2000. Cofactor dynamics and sufficiency in estrogen receptor-regulated transcription. Cell **103:**843–852. http://dx.doi.org/10.1016/S0092-8674(00)00188-4.
9. **van Driel R, Fransz PF, Verschure PJ.** 2003. The eukaryotic genome: a system regulated at different hierarchical levels. J. Cell Sci. **116:**4067–4075. http://dx.doi.org/10.1242/jcs.00779.
10. **Hurst LD, Pal C, Lercher MJ.** 2004. The evolutionary dynamics of eukaryotic gene order. Nat. Rev. Genet. **5:**299–310. http://dx.doi.org/10.1038/nrg1319.
11. **Li Q, Barkess G, Qian H.** 2006. Chromatin looping and the probability of transcription. Trends Genet. **22:**197–202. http://dx.doi.org/10.1016/j.tig.2006.02.004.
12. **Carvajal JJ, Keith A, Rigby PW.** 2008. Global transcriptional regulation of the locus encoding the skeletal muscle determination genes Mrf4 and Myf5. Genes Dev. **22:**265–276. http://dx.doi.org/10.1101/gad.442408.
13. **Tang Y, Huang Y, Shen W, Liu G, Wang Z, Tang XB, Feng DX, Liu DP, Liang CC.** 2008. Cluster specific regulation pattern of upstream regulatory elements in human alpha- and beta-globin gene clusters. Exp. Cell Res. **314:**115–122. http://dx.doi.org/10.1016/j.yexcr.2007.08.014.
14. **Carroll JS, Brown M.** 2006. Estrogen receptor target gene: an evolving concept. Mol. Endocrinol. **20:**1707–1714. http://dx.doi.org/10.1210/me.2005-0334.
15. **Fullwood MJ, Liu MH, Pan YF, Liu J, Xu H, Mohamed YB, Orlov YL, Velkov S, Ho A, Mei PH, Chew EG, Huang PY, Welboren WJ, Han Y, Ooi HS, Ariyaratne PN, Vega VB, Luo Y, Tan PY, Choy PY, Wansa KD, Zhao B, Lim KS, Leow SC, Yow JS, Joseph R, Li H, Desai KV, Thomsen JS, Lee YK, Karuturi RK, Herve T, Bourque G, Stunnenberg HG, Ruan X, Cacheux-Rataboul V, Sung WK, Liu ET, Wei CL, Cheung E, Ruan Y.** 2009. An oestrogen-receptor-alpha-bound human chromatin interactome. Nature **462:**58–64. http://dx.doi.org/10.1038/nature08497.
16. **Zaret KS, Carroll JS.** 2011. Pioneer transcription factors: establishing competence for gene expression. Genes Dev. **25:**2227–2241. http://dx.doi.org/10.1101/gad.176826.111.
17. **Carroll JS, Meyer CA, Song J, Li W, Geistlinger TR, Eeckhoute J, Brodsky AS, Keeton EK, Fertuck KC, Hall GF, Wang Q, Bekiranov S, Sementchenko V, Fox EA, Silver PA, Gingeras TR, Liu XS, Brown M.** 2006. Genome-wide analysis of estrogen receptor binding sites. Nat. Genet. **38:**1289–1297. http://dx.doi.org/10.1038/ng1901.
18. **Tan SK, Lin ZH, Chang CW, Varang V, Chng KR, Pan YF, Yong EL, Sung WK, Cheung E.** 2011. AP-2γ regulates oestrogen receptor-mediated long-range chromatin interaction and gene transcription. EMBO J. **30:**2569–2581. http://dx.doi.org/10.1038/emboj.2011.151.
19. **Magnani L, Ballantyne EB, Zhang X, Lupien M.** 2011. PBX1 genomic pioneer function drives ERα signaling underlying progression in breast cancer. PLoS Genet. **7:**e1002368. http://dx.doi.org/10.1371/journal.pgen.1002368.
20. **Lupien M, Eeckhoute J, Meyer CA, Wang Q, Zhang Y, Li W, Carroll JS, Liu XS, Brown M.** 2008. FoxA1 translates epigenetic signatures into enhancer-driven lineage-specific transcription. Cell **132:**958–970. http://dx.doi.org/10.1016/j.cell.2008.01.018.
21. **Magnani L, Eeckhoute J, Lupien M.** 2011. Pioneer factors: directing transcriptional regulators within the chromatin environment. Trends Genet. **27:**465–474. http://dx.doi.org/10.1016/j.tig.2011.07.002.
22. **Serandour AA, Avner S, Percevault F, Demay F, Bizot M, Lucchetti-Miganeh C, Barloy-Hubler F, Brown M, Lupien M, Métivier R, Salbert G, Eeckhoute J.** 2011. Epigenetic switch involved in activation of pioneer factor FOXA1-dependent enhancers. Genome Res. **21:**555–565. http://dx.doi.org/10.1101/gr.111534.110.
23. **Reid G, Hubner MR, Metivier R, Brand H, Denger S, Manu D, Beaudouin J, Ellenberg J, Gannon F.** 2003. Cyclic, proteasome-mediated

turnover of unliganded and liganded ERalpha on responsive promoters is an integral feature of estrogen signaling. Mol. Cell **11:**695–707. http://dx.doi.org/10.1016/S1097-2765(03)00090-X.
24. **Watrin E, Legagneux V.** 2005. Contribution of hCAP-D2, a non-SMC subunit of condensin I, to chromosome and chromosomal protein dynamics during mitosis. Mol. Cell. Biol. **25:**740–750. http://dx.doi.org/10.1128/MCB.25.2.740-750.2005.
25. **Vekhoff P, Ceccaldi A, Polverari D, Pylouster J, Pisano C, Arimondo PB.** 2008. Triplex formation on DNA targets: how to choose the oligonucleotide. Biochemistry **47:**12277–12289. http://dx.doi.org/10.1021/bi801087g.
26. **Eimer S, Dugay F, Airiau K, Avril T, Quillien V, Belaud-Rotureau MA, Belloc F.** 2012. Cyclopamine cooperates with EGFR inhibition to deplete stem-like cancer cells in glioblastoma-derived spheroid cultures. Neuro. Oncol. **14:**1441–1451. http://dx.doi.org/10.1093/neuonc/nos266.
27. **Zack GW, Rogers WE, Latt SA.** 1977. Automatic measurement of sister chromatid exchange frequency. J. Histochem. Cytochem. **25:**741–753. http://dx.doi.org/10.1177/25.7.70454.
28. **Otsu N.** 1979. A threshold selection method from gray-level histograms. IEEE Trans. Syst. Man Cyber. **9:**62–66. http://dx.doi.org/10.1109/TSMC.1979.4310076.
29. **Meyer F.** 1994. Topographic distance and watershed lines. Signal Processing **38:**113–125. http://dx.doi.org/10.1016/0165-1684(94)90060-4.
30. **Sbalzarini IF, Koumoutsakos P.** 2005. Feature point tracking and trajectory analysis for video imaging in cell biology. J. Struct. Biol. **151:**182–195. http://dx.doi.org/10.1016/j.jsb.2005.06.002.
31. **Benjamini Y, Hochberg Y.** 1995. Controlling the false discovery rate: a practical and powerful approach to multiple testing. J. R. Stat. Soc. Series B Stat. Methodol. **57:**289–300.
32. **Giresi PG, Kim J, McDaniell RM, Iyer VR, Lieb JD.** 2007. FAIRE (formaldehyde-assisted isolation of regulatory elements) isolates active regulatory elements from human chromatin. Genome Res. **17:**877–885. http://dx.doi.org/10.1101/gr.5533506.
33. **Song JS, Johnson WE, Zhu X, Zhang X, Li W, Manrai AK, Liu JS, Chen R, Liu XS.** 2007. Model-based analysis of two-color arrays (MA2C). Genome Biol. **8:**R178. http://dx.doi.org/10.1186/gb-2007-8-8-r178.
34. **Johnson WE, Li W, Meyer CA, Gottardo R, Carroll JS, Brown M, Liu XS.** 2006. Model-based analysis of tiling-arrays for ChIP-chip. Proc. Natl. Acad. Sci. U. S. A. **103:**12457–12462. http://dx.doi.org/10.1073/pnas.0601180103.
35. **Blankenberg D, Taylor J, Schenck I, He J, Zhang Y, Ghent M, Veeraraghavan N, Albert I, Miller W, Makova KD, Hardison RC, Nekrutenko A.** 2007. A framework for collaborative analysis of ENCODE data: making large-scale analyses biologist-friendly. Genome Res. **17:**960–964. http://dx.doi.org/10.1101/gr.5578007.
36. **Langmead B, Trapnell C, Pop M, Salzberg SL.** 2009. Ultrafast and memory-efficient alignment of short DNA sequences to the human genome. Genome Biol. **10:**R25. http://dx.doi.org/10.1186/gb-2009-10-3-r25.
37. **Li H, Handsaker B, Wysoker A, Fennell T, Ruan J, Homer N, Marth G, Abecasis G, Durbin R, 1000 Genome Project Data Processing Subgroup.** 2009. The sequence alignment/Map format and SAMtools. Bioinformatics **25:**2078–2079. http://dx.doi.org/10.1093/bioinformatics/btp352.
38. **Zhang Y, Liu T, Meyer CA, Eeckhoute J, Johnson DS, Bernstein BE, Nusbaum C, Myers RM, Brown M, Li W, Liu XS.** 2008. Model-based analysis of ChIP-Seq (MACS). Genome Biol. **9:**R137. http://dx.doi.org/10.1186/gb-2008-9-9-r137.
39. **Sérandour AA, Avner S, Oger F, Bizot M, Percevault F, Lucchetti-Miganeh C, Palierne G, Gheeraert C, Barloy-Hubler F, Péron CL, Madigou T, Durand E, Froguel P, Staels B, Lefebvre P, Métivier R, Eeckhoute J, Salbert G.** 2012. Dynamic hydroxymethylation of deoxyribonucleic acid marks differentiation-associated enhancers. Nucleic Acids Res. **40:**8255–8265. http://dx.doi.org/10.1093/nar/gks595.
40. **Gondor A, Rougier C, Ohlsson R.** 2008. High-resolution circular chromosome conformation capture assay. Nat. Protoc. **3:**303–313. http://dx.doi.org/10.1038/nprot.2007.540.
41. **Shannon P, Markiel A, Ozier O, Baliga NS, Wang JT, Ramage D, Amin N, Schwikowski B, Ideker T.** 2003. Cytoscape: a software environment for integrated models of biomolecular interaction networks. Genome Res. **13:**2498–2504. http://dx.doi.org/10.1101/gr.1239303.
42. **Arvidsson S, Kwasniewski M, Riano-Pachon DM, Mueller-Roeber B.** 2008. QuantPrime—a flexible tool for reliable high-throughput primer design for quantitative PCR. BMC Bioinformatics **9:**465. http://dx.doi.org/10.1186/1471-2105-9-465.
43. **Saeed AI, Sharov V, White J, Li J, Liang W, Bhagabati N, Braisted J, Klapa M, Currier T, Thiagarajan M, Sturn A, Snuffin M, Rezantsev A, Popov D, Ryltsov A, Kostukovich E, Borisovsky I, Liu Z, Vinsavich A, Trush V, Quackenbush J.** 2003. TM4: a free, open-source system for microarray data management and analysis. Biotechniques **34:**374–378.
44. **Barrett T, Troup DB, Wilhite SE, Ledoux P, Rudnev D, Evangelista C, Kim IF, Soboleva A, Tomashevsky M, Marshall KA, Phillippy KH, Sherman PM, Muertter RN, Edgar R.** 2009. NCBI GEO: archive for high-throughput functional genomic data. Nucleic Acids Res. **37:**D885–D890. http://dx.doi.org/10.1093/nar/gkn764.
45. **Moggs JG, Murphy TC, Lim FL, Moore DJ, Stuckey R, Antrobus K, Kimber I, Orphanides G.** 2005. Anti-proliferative effect of estrogen in breast cancer cells that re-express ERalpha is mediated by aberrant regulation of cell cycle genes. J. Mol. Endocrinol. **34:**535–551. http://dx.doi.org/10.1677/jme.1.01677.
46. **Nott SL, Huang Y, Li X, Fluharty BR, Qiu X, Welshons WV, Yeh S, Muyan M.** 2009. Genomic responses from the estrogen-responsive element-dependent signaling pathway mediated by estrogen receptor alpha are required to elicit cellular alterations. J. Biol. Chem. **284:**15277–15288. http://dx.doi.org/10.1074/jbc.M900365200.
47. **Kong SL, Li G, Loh SL, Sung W-K, Liu ET.** 2011. Cellular reprogramming by the conjoint action of ERα, FOXA1, and GATA3 to a ligand-inducible growth state. Mol. Syst. Biol. **7:**526. http://dx.doi.org/10.1038/msb.2011.59.
48. **Chinery R, Williamson J, Poulsom R.** 1996. The gene encoding human intestinal trefoil factor (TFF3) is located on chromosome 21q22.3 clustered with other members of the trefoil peptide family. Genomics **32:**281–284. http://dx.doi.org/10.1006/geno.1996.0117.
49. **Hah N, Danko CG, Core L, Waterfall JJ, Siepel A, Lis JT, Kraus WL.** 2011. A rapid, extensive, and transient transcriptional response to estrogen signaling in breast cancer cells. Cell **145:**622–634. http://dx.doi.org/10.1016/j.cell.2011.03.042.
50. **Hah N, Murakami S, Nagari A, Danko C, Kraus WL.** 2013. Enhancer transcripts mark active estrogen receptor binding sites. Genome Res. http://dx.doi.org/10.1101/gr.152306.112.
51. **Li W, Notani D, Ma Q, Tanasa B, Nunez E, Chen AY, Merkurjev D, Zhang J, Ohgi K, Song X, Oh S, Kim HS, Glass CK, Rosenfeld MG.** 2013. Functional roles of enhancer RNAs for oestrogen-dependent transcriptional activation. Nature **498:**516–520. http://dx.doi.org/10.1038/nature12210.
52. **Hsu PY, Hsu HK, Singer GA, Yan PS, Rodriguez BA, Liu JC, Weng YI, Deatherage DE, Chen Z, Pereira JS, Lopez R, Russo J, Wang Q, Lamartiniere CA, Nephew KP, Huang TH.** 2010. Estrogen-mediated epigenetic repression of large chromosomal regions through DNA looping. Genome Res. **20:**733–744. http://dx.doi.org/10.1101/gr.101923.109.
53. **Schmidt D, Schwalie PC, Ross-Innes CS, Hurtado A, Brown GD, Carroll JS, Flicek P, Odom DT.** 2010. A CTCF-independent role for cohesin in tissue-specific transcription. Genome Res. **20:**578–588. http://dx.doi.org/10.1101/gr.100479.109.
54. **McGuffie EM, Catapano CV.** 2002. Design of a novel triple helix-forming oligodeoxyribonucleotide directed to the major promoter of the c-myc gene. Nucleic Acids Res. **30:**2701–2709. http://dx.doi.org/10.1093/nar/gkf376.
55. **Jain A, Magistri M, Napoli S, Carbone GM, Catapano CV.** 2010. Mechanisms of triplex DNA-mediated inhibition of transcription initiation in cells. Biochimie **92:**317–320. http://dx.doi.org/10.1016/j.biochi.2009.12.012.
56. **Knauert MP, Glazer PM.** 2001. Triplex forming oligonucleotides: sequence-specific tools for gene targeting. Hum. Mol. Genet. **10:**2243–2251. http://dx.doi.org/10.1093/hmg/10.20.2243.
57. **Kalish JM, Glazer PM.** 2005. Targeted genome modification via triple helix formation. Ann. N. Y. Acad. Sci. **1058:**151–161. http://dx.doi.org/10.1196/annals.1359.023.
58. **Hurtado A, Holmes KA, Ross-Innes CS, Schmidt D, Carroll JS.** 2011. FOXA1 is a key determinant of estrogen receptor function and endocrine response. Nat. Genet. **43:**27–33. http://dx.doi.org/10.1038/ng.730.
59. **Eeckhoute J, Keeton EK, Lupien M, Krum SA, Carroll JS, Brown M.** 2007. Positive cross-regulatory loop ties GATA-3 to estrogen receptor alpha expression in breast cancer. Cancer Res. **67:**6477–6483. http://dx.doi.org/10.1158/0008-5472.CAN-07-0746.
60. **Theodorou V, Stark R, Menon S, Carroll JS.** 2013. GATA3 acts upstream of FOXA1 in mediating ESR1 binding by shaping enhancer accessibility. Genome Res. **23:**12–22. http://dx.doi.org/10.1101/gr.139469.112.

61. **Nora EP, Lajoie BR, Schulz EG, Giorgetti L, Okamoto I, Servant N, Piolot T, van Berkum NL, Meisig J, Sedat J, Gribnau J, Barillot E, Blüthgen N, Dekker J, Heard E.** 2012. Spatial partitioning of the regulatory landscape of the X-inactivation centre. Nature **485:**381–385. http://dx.doi.org/10.1038/nature11049.
62. **Gibcus JH, Dekker J.** 2013. The hierarchy of the 3D genome. Mol. Cell **49:**773–782. http://dx.doi.org/10.1016/j.molcel.2013.02.011.
63. **Nora EP, Dekker J, Heard E.** 2013. Segmental folding of chromosomes: a basis for structural and regulatory chromosomal neighborhoods? Bioessays **35:**818–828. http://dx.doi.org/10.1002/bies.201300040.
64. **Schaaf CA, Kwak H, Koenig A, Misulovin Z, Gohara DW, Watson A, Zhou Y, Lis JT, Dorsett D.** 2013. Genome-wide control of RNA polymerase II activity by cohesin. PLoS Genet. **9:**e1003382. http://dx.doi.org/10.1371/journal.pgen.1003382.
65. **Li Y, Huang W, Niu L, Umbach DM, Covo S, Li L.** 2013. Characterization of constitutive CTCF/cohesin loci: a possible role in establishing topological domains in mammalian genomes. BMC Genomics **14:**553. http://dx.doi.org/10.1186/1471-2164-14-553.
66. **DeMare LE, Leng J, Cotney J, Reilly SK, Yin J, Sarro R, Noonan JP.** 2013. The genomic landscape of cohesin-associated chromatin interactions. Genome Res. **23:**1224–1234. http://dx.doi.org/10.1101/gr.156570.113.
67. **Sanyal A, Lajoie BR, Jain G, Dekker J.** 2012. The long-range interaction landscape of gene promoters. Nature **489:**109–113. http://dx.doi.org/10.1038/nature11279.
68. **Zhang Y, Liang J, Li Y, Xuan C, Wang F, Wang D, Shi L, Zhang D, Shang Y.** 2010. CCCTC-binding factor acts upstream of FOXA1 and demarcates the genomic response to estrogen. J. Biol. Chem. **285:**28604–28613. http://dx.doi.org/10.1074/jbc.M110.149658.
69. **Faure AJ, Schmidt D, Watt S, Schwalie PC, Wilson MD, Xu H, Ramsay RG, Odom DT, Flicek P.** 2012. Cohesin regulates tissue-specific expression by stabilizing highly occupied cis-regulatory modules. Genome Res. **22:**2163–2175. http://dx.doi.org/10.1101/gr.136507.111.
70. **Gavrilov AA, Gushchanskaya ES, Strelkova O, Zhironkina O, Kireev II, Iarovaia OV, Razin SV.** 2013. Disclosure of a structural milieu for the proximity ligation reveals the elusive nature of an active chromatin hub. Nucleic Acids Res. **41:**3563–3575. http://dx.doi.org/10.1093/nar/gkt067.
71. **Kagey MH, Newman JJ, Bilodeau S, Zhan Y, Orlando DA, van Berkum NL, Ebmeier CC, Goossens J, Rahl PB, Levine SS, Taatjes DJ, Dekker J, Young RA.** 2010. Mediator and cohesin connect gene expression and chromatin architecture. Nature **467:**430–435. http://dx.doi.org/10.1038/nature09380.
72. **Saramäki A, Diermeier S, Kellner R, Laitinen H, Vaïsänen S, Carlberg C.** 2009. Cyclical chromatin looping and transcription factor association on the regulatory regions of the p21 (CDKN1A) gene in response to 1alpha,25-dihydroxyvitamin D3. J. Biol. Chem. **284:**8073–8082. http://dx.doi.org/10.1074/jbc.M808090200.
73. **Wang J, Lan X, Hsu PY, Hsu HK, Huang K, Parvin J, Huang TH, Jin VX.** 2013. Genome-wide analysis uncovers high frequency, strong differential chromosomal interactions and their associated epigenetic patterns in E2-mediated gene regulation. BMC Genomics **14:**70. http://dx.doi.org/10.1186/1471-2164-14-70.
74. **Eeckhoute J, Métivier R, Salbert G.** 2009. Defining specificity of transcription factor regulatory activities. J. Cell Sci. **122:**4027–4034. http://dx.doi.org/10.1242/jcs.054916.
75. **Attanasio C, Nord AS, Zhu Y, Blow MJ, Li Z, Liberton DK, Morrison H, Plajzer-Frick I, Holt A, Hosseini R, Phouanenavong S, Akiyama JA, Shoukry M, Afzal V, Rubin EM, FitzPatrick DR, Ren B, Hallgrímsson B, Pennacchio LA, Visel A.** 2013. Fine tuning of craniofacial morphology by distant-acting enhancers. Science **342:**1241006. http://dx.doi.org/10.1126/science.1241006.
76. **Lupien M, Meyer CA, Bailey ST, Eeckhoute J, Cook J, Westerling T, Zhang X, Carroll JS, Rhodes DR, Liu XS, Brown M.** 2010. Growth factor stimulation induces a distinct ER(alpha) cistrome underlying breast cancer endocrine resistance. Genes Dev. **24:**2219–2227. http://dx.doi.org/10.1101/gad.1944810.
77. **Gotea V, Visel A, Westlund JM, Nobrega MA, Pennacchio LA, Ovcharenko I.** 2010. Homotypic clusters of transcription factor binding sites are a key component of human promoters and enhancers. Genome Res. **20:**565–577. http://dx.doi.org/10.1101/gr.104471.109.
78. **Nielsen PE.** 2010. Gene targeting and expression modulation by peptide nucleic acids (PNA). Curr. Pharm. Des. **16:**3118–3123. http://dx.doi.org/10.2174/138161210793292546.
79. **Brunet E, Corgnali M, Cannata F, Perrouault L, Giovannangeli C.** 2006. Targeting chromosomal sites with locked nucleic acid-modified triplex-forming oligonucleotides: study of efficiency dependence on DNA nuclear environment. Nucleic Acids Res. **34:**4546–4553. http://dx.doi.org/10.1093/nar/gkl630.
80. **Moreno PM, Geny S, Pabon YV, Bergquist H, Zaghloul EM, Rocha CS, Oprea II, Bestas B, Andaloussi SE, Jørgensen PT, Pedersen EB, Lundin KE, Zain R, Wengel J, Smith CI.** 2013. Development of bis-locked nucleic acid (bisLNA) oligonucleotides for efficient invasion of supercoiled duplex DNA. Nucleic Acids Res. **41:**3257–3273. http://dx.doi.org/10.1093/nar/gkt007.
81. **Nicol JW, Helt GA, Blanchard SG, Jr, Raja A, Loraine AE.** 2009. The Integrated Genome Browser: free software for distribution and exploration of genome-scale datasets. Bioinformatics **25:**2730–2731. http://dx.doi.org/10.1093/bioinformatics/btp472.